A Network Scission Model for Wormlike Micellar Solutions I: Model Formulation and Homogeneous Flow Predictions

Paula A. Vasquez, L. Pamela Cook, Gareth McKinley

November 6, 2006

Abstract

In this paper a network model for wormlike micellar solutions is presented which incorporates scission and reforming of the chains, based on a discrete version of Cates' theory. Specifically we consider two elastically active Hookean species: long chains which can break to form short chains which themselves can recombine to form a long chain. The chains undergo rupture at a rate dependent on the local elongation and deformation rate. This two species model, developed for an understanding of inhomogeneous flows, is examined in this paper in various deformations; steady state shear flow, step strain, extension, and linear small angle oscillatory flow in homogeneous conditions. The values of the model parameters and their effects on the flow predictions are examined.

1 Introduction

Wormlike micelles, also known as living polymers, have been the center of numerous theoretical and experimental studies, see for example the reviews [1], [2]. Unlike typical polymers these long macromolecular assemblies can break and reform continuously, showing distinctive behaviors under different deformation conditions. Observations in small amplitude oscillatory shear (SAOS) flows show that under certain conditions the linear viscoelastic response is primarily a single mode Maxwell response [3], [4]. Specifically, if we denote τ_{break} as the expected time for breakage of the micelle, and $\tau_{\text{reptation}}$ as the expected time for a micelle to reptate out of its entanglements, when $\tau_{\text{break}} << \tau_{\text{reptation}}$, Cates, [5], showed that wormlike micellar mixtures have a single mode Maxwellian response in the linear viscoelastic

regime, with a second mode important only at high frequencies. He also showed that the time scale associated with this first, dominant, mode is $\tau_{\text{eff}} = (\tau_{\text{reptation}}\tau_{\text{break}})^{\frac{1}{2}}$ [5], [6]. In steady state shear experiments, at small shear rates, $\dot{\gamma} < \dot{\gamma}_1$, and large shear rates, $\dot{\gamma} > \dot{\gamma}_2$, these mixtures exhibit a linear dependence of the stress on the shear rate. However, given the right conditions in concentration, salinity, and temperature [7], a stress plateau in an intermediate shear-rate region, $\dot{\gamma}_1 < \dot{\gamma} < \dot{\gamma}_2$, is observed in the flow curve and, in these cases, experiments in a circular Couette cell show the formation of two primary 'shear bands', a high shear rate region near the inner or moving wall connected to a low shear rate region near the outer or fixed wall [8], [9], [10].

In uniaxial extension flows experiments have shown a plateau in the extensional viscosity for small extensional rates, followed by a sharp extensional thickening and, at a critical elongational rate, an extensional thinning. [11]

In step strain these mixtures show a factorization of the shear stress as $\sigma_{r\theta} = \gamma\, G_0\, g(t)\, h(\gamma)$ where $G(t) = G_0 g(t)$ is the stress relaxation modulus and $h(\gamma)$ the damping function. Experiments have shown that $G(t)$ can be well described by single exponential relaxation $G(t) = G_0 e^{-t/\lambda}$. The damping function may have a more complex response. Experiments by Brown *et. al.* [12] on a CTAB/NaSal system show a strain-hardening followed by a strain-softening. Recent experiments with a CPyCl/NaSal solution show a monotonic softening response similar to that described by the Doi-Edwards model [13]. Additionally, experiments show that the Lodge-Meissner relation is obeyed up to strains of $\gamma_0 \sim 8$ [13].

The present work presents a constitutive model to describe the flow of wormlike micellar solutions under these different deformation conditions and details the predictions and parameter dependence of the model. The model includes scission and reformation effects.

Various approaches have been taken in modeling wormlike micellar solutions. Cates [14] introduced reaction dynamics to account for the reversible breaking and reforming of the micellar chains. In his model there are two different time scales, the reptation time and the breaking time. Although experiments have shown good agreement with his model, especially in linear deformations, that model still fails to predict stress overshoot in the start up of steady shear [6] and to our knowledge no calculations in extensional flow have been done for that model. Other authors have combined dumbbell models for elastic chains and network theory by introducing creation and destruction terms in the evolution equation of the dumbbells [15]-[16]. Different forms of these breaking and reforming terms have been considered.

Bautista *et. al.* [17] developed a single species model based on a codeformational Maxwell constitutive equation and included a kinetic equation governing the relaxation time to account for the dependence of the breakage rate on the shear rate. This particular version of their model predicts a multivalued shear stress versus shear rate curve and hence one expects that the model will demonstrate shear banding.

Two species models have been considered to describe associative polymeric networks. These mixtures do not typically exhibit shear banding, but these models do incorporated two species in a network with attachment and detachment of strands. Using Brownian dynamics simulations to evaluated the rheological behavior of reversible polymeric networks, Van den Brule *et. al.* [18] assumed that the probability of attachment to the network is proportional to the stretch of the dumbbell. They introduced a FENE-like term in the probability of detachment to account for the fact that during flow a chain has a higher probability of detaching once it becomes more fully stretched. Brownian dynamics were also used in the work of Hernandez-Cifre *et. al.* [16] to simulate reversible polymeric networks, they considered two separate species, one representing active chains connected to the network by both ends, and the other representing dangling chains connected to the network by one end only. In their work, disassociation from the network was an exponential function of stress and, by using the same form of the association rate as van den Brule *et. al.*, they were able to predict shear thickening. Tripathi *et. al.* [19] in their two species network model for associative polymers derived a destruction rate for the bridging chains which is proportional to a power of the Warner spring function, the power is related to the molecular weight of the species. In their work the creation rate of the bridging chains was proportional to a function of the shear rate and stress.

Single species bead-spring models based on the Johnson-Segalmann constitutive equation were considered by Olmsted and collaborators. In these models the number density of the species was kept fixed and numerical studies were carried out with and without non-local diffusion terms, [20], [21], [22]. A similar model but with addition of variable density was considered in [23], [24]. These models result in a nonmonotone stress-strain rate curve under homogeneous flow conditions. Under inhomogeneous flow conditions, with the addition of a viscous solvent and the incorporation of stress diffusion terms, these models predict a stress plateau in the flow curve for a range of shear rates. Numerical studies have shown that, without diffusion, this steady state solution depends on the flow history [20]. For shear rates within the plateau region, these models predict shear banding in the velocity profiles across the gap in a cylindrical Couette geometry. Such models

are phenomenological, that is they do not relate directly to the dynamics of the micellar system. Additionally, the Johnson-Segalman model predicts a singularity in the Trouton ratio at a finite elongational rate and exhibits a nonphysical negative damping in rapid step strain deformation [25]. Experiments using NMR microscopy [26] and small-angle neutron scattering [27] have also shown that for a model to be able to accurately describe the highly non-linear behavior of some wormlike micellar solutions, it should include local effects in the orientation and dynamics of the molecules, as opposed to a bulk average of the properties. For these reasons alternative models, tied to the physics of the micellar breakage and reforming processes, should be considered.

The present approach is based on a discrete version of Cates' original reversible breaking theory. In contrast to Cates' model in which reptation theory was used, the breaking and reforming dynamics in this model are incorporated into network theory in which we follow elastic segments of wormy micelles between entanglement points. In the present approach two different species are considered, one of length L that breaks in the middle to form two of length $L/2$. These recombine to form one species of length L as shown in Figure 1.

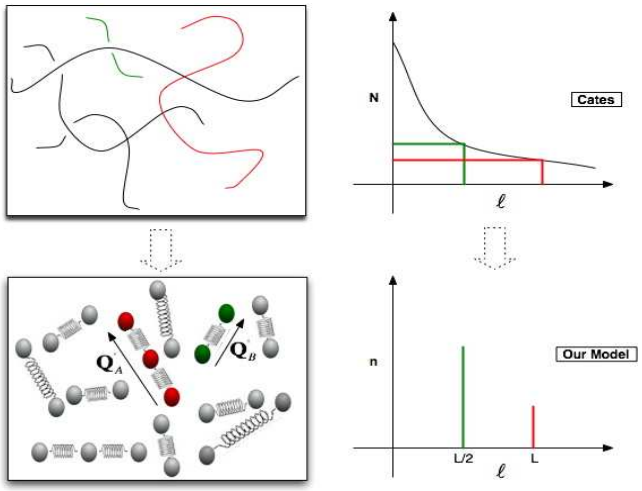

Figure 1: Micellar network: a. Cates' model with a continuous distribution of lengths $N(L)$. b . Our discrete two species model.

In this paper we formulate the model and consider predictions under different deformation conditions assuming homogeneous flow. In Section 2

we present the formulation and non-dimensionalization of our model. In Section 3 the governing equations describing steady and transient shear flow in a cylindrical Couette geometry and in uniaxial extensional flows are presented. Section 4 deals with analysis of the model in the linear viscoelastic regime, specifically small amplitude oscillation. Also, a first look at the model parameters and their effects on the model predictions and in particular on the magnitude of the zero shear rate viscosity are studied. In Section 5 nonlinear material functions in step strain, and steady homogenous shear and elongational flow are studied. The dependency of the material functions on model parameters such as the equilibrium number density of each species and the breakage rate are explored. Part II of this paper [13], consists of a detailed comparison of experiments with the predictions of the model and parameter selection for the model in agreement with experiments. A third paper, Part III [28], analyzes the model computationally in steady and transient inhomogeneous shearing flows.

2 Formulation of the Model

In the model presented here we simplify Cates' dynamics by considering only two species of wormlike micelles. We consider species A, which are chains of length L units that break at the middle to form chains of length $L/2$ units, denoted species B. Analogously, the short chains can join at their ends to reform into one long chain. This discrete dynamics is opposed to Cates' theory in which chains can break with equal probability at any point along their length, and in which chains of any length can join to form a longer chain. This simplification of Cates' breakage dynamics allows us to understand the species interaction, to examine the model in a variety of nonlinear flow conditions, and in particular, to develop a theory which consistently captures the spatial variations in the number density of each species. This is key to understanding the experimental behavior of wormlike micellar solutions and the selection of the stress at which these solutions show shear banding [29]. One effect the continuous, versus the discrete, dynamics has on our results is that by allowing the chains to break at any point, the rate of breakage is effectively increased and the breakage time correspondingly decreased.

Let $\Psi_A^{'}(\mathbf{r}', \mathbf{Q}', t')$, $\Psi_B^{'}(\mathbf{r}', \mathbf{Q}', t')$ represent the number density distribution of each species in space, configuration space and time. Here $\mathbf{Q}^{'}$ is the

end to end vector of the chain. Then,

$$n'_\alpha(\mathbf{r}', t') = \int \Psi'_\alpha d\mathbf{Q}'$$

represents the dimensional number density of species α as a function of space and time. Here and throughout this paper primes represent dimensional variables.

The equations governing the configuration density function, using network theory coupled with bead-spring kinetics, and assuming Hookean forces, can be obtained generalizing techniques introduced by Bird, Curtis, Armstrong and Hassager, [30], [31], [32] and used in [23], [24], to a two species model:

$$\Psi'_{A,t'} + \nabla_{\mathbf{r}'} \cdot \left(\mathbf{v}'_A \Psi'_A\right) + \nabla_{\mathbf{Q}'} \left(\mathbf{Q}' \cdot \nabla \mathbf{v}'_A\right) \Psi'_A - \nabla_{\mathbf{r}'} \cdot \frac{kT}{2\zeta_A} \nabla_{\mathbf{r}'} \Psi'_A$$
$$+ \nabla_{\mathbf{Q}'} \cdot \frac{2H_A}{\zeta_A} \mathbf{Q}' \Psi'_A - \nabla_{\mathbf{Q}'} \frac{2kT}{\zeta_A} \nabla_{\mathbf{Q}'} \Psi'_A = \frac{c'_B}{2} \Psi'_B * \Psi'_B - c'_A \Psi'_A \qquad (1a)$$

$$\Psi'_{B,t'} + \nabla_{\mathbf{r}'} \cdot \left(\mathbf{v}'_B \Psi'_B\right) + \nabla_{\mathbf{Q}'} \left(\mathbf{Q}' \cdot \nabla \mathbf{v}'_B\right) \Psi'_B - \nabla_{\mathbf{r}'} \cdot \frac{kT}{2\zeta_B} \nabla_{\mathbf{r}'} \Psi'_B$$
$$+ \nabla_{\mathbf{Q}'} \cdot \frac{2H_B}{\zeta_B} \mathbf{Q}' \Psi'_B - \nabla_{\mathbf{Q}'} \frac{2kT}{\zeta_B} \nabla_{\mathbf{Q}'} \Psi'_B = -c'_B \Psi'_B * \Psi'_B + 2c'_A \Psi'_A \qquad (1b)$$

In these equations k is the Boltzmann constant, T is temperature, ζ_α represents the drag coefficient of the species α, ${c_A}'$ represents the dimensional breakage rate, ${c_B}'$ represents the dimensional reforming rate per micelle, and H_α is the spring constant or elasticity of the α^{th} species.

The flux of species A and B relative to the main flow is given by

$$\mathbf{j}'_A = -\frac{kT}{\zeta_A} \nabla' \rho'_A + \frac{2mH_A}{\zeta_A} \nabla' \cdot \{\mathbf{Q}'\mathbf{Q}'\}_A, \qquad (2a)$$

$$\mathbf{j}'_B = -\frac{kT}{\zeta_B} \nabla' \rho'_B + \frac{mH_B}{\zeta_B} \nabla' \cdot \{\mathbf{Q}'\mathbf{Q}'\}_B. \qquad (2b)$$

The second term on the right hand side of Equations (2) arises from assuming there is a finite spatial extent for the dumbbell and the mass is distributed at the two ends, one bead at $(\mathbf{r}' + \frac{\mathbf{Q}'}{2}, \mathbf{Q}', t')$ and the other at $(\mathbf{r}' - \frac{\mathbf{Q}'}{2}, \mathbf{Q}', t')$ [23], [31], [32].

By integrating the Smoluchowski equations (1) over $\mathbf{Q}'$, with $\rho'_A = 4mn'_A$

and $\rho'_B = 2mn'_B$, we obtain the evolution equations governing the number densities of each species,

$$\frac{Dn'_A}{Dt'} = -\frac{\nabla' \cdot \mathbf{j}'_A}{4m} + \frac{c_B{}'}{2} n'^2_B - c_A{}' n'_A, \tag{3a}$$

$$\frac{Dn'_B}{Dt'} = -\frac{\nabla' \cdot \mathbf{j}'_B}{2m} - c_B{}' n'^2_B + 2c_A{}' n'_A. \tag{3b}$$

The functional form of the reaction rates, $c_A{}', c_B{}'$, for the breaking and reforming of the chains will be discussed in Section 2.3. For now we assume they are functions of the average extension of the chains and the shear rate:

$$c_A{}' \left(n'_A, \{\mathbf{Q}'\mathbf{Q}'\}_A, \dot{\boldsymbol{\gamma}}' \right), \quad c_B{}' \left(n'_B, \{\mathbf{Q}'\mathbf{Q}'\}_B, \dot{\boldsymbol{\gamma}}' \right).$$

Substituting for the flux from equations (2) into (3), the equations for the number density for each species become

$$\frac{Dn'_A}{Dt'} = 2D_A \nabla'^2 n'_A - \frac{D_A H_A}{kT} \nabla'\nabla' : \{\mathbf{Q}'\mathbf{Q}'\}_A + \frac{c_B{}'}{2} n'^2_B - c_A{}' n'_A \tag{4a}$$

$$\frac{Dn'_B}{Dt'} = 2D_B \nabla'^2 n'_B - \frac{D_B H_B}{kT} \nabla'\nabla' : \{\mathbf{Q}'\mathbf{Q}'\}_B - c_B{}' n'^2_B + 2c_A{}' n'_A \tag{4b}$$

Here the diffusivities of the A and B chains are $D_A = \frac{kT}{2\zeta_A}, D_B = \frac{kT}{2\zeta_B}$, respectively. The stress associated with the α^{th} species is related to the second moment of the distribution by

$$\{\mathbf{Q}'\mathbf{Q}'\}_\alpha = \int \mathbf{Q}'\mathbf{Q}'\Psi'_\alpha d\mathbf{Q}'. \tag{5}$$

Then multiplying the distribution equations (1) by $\mathbf{Q}'\mathbf{Q}'$ and integrating over the configuration space, $d\mathbf{Q}'$, we find the equations for the second moment of each species:

$$\{\mathbf{Q}'\mathbf{Q}'\}_{A(1')} + \frac{4H_A}{\zeta_A}\{\mathbf{Q}'\mathbf{Q}'\}_A - \frac{4n'_A kT}{\zeta_A}\mathbf{I} - D_A \nabla'^2 \{\mathbf{Q}'\mathbf{Q}'\}_A = \frac{c_B{}'}{2}\{\mathbf{Q}'\mathbf{Q}'\}_B n'_B - c_A{}'\{\mathbf{Q}'\mathbf{Q}'\}_A, \tag{6a}$$

$$\{\mathbf{Q}'\mathbf{Q}'\}_{B(1')} + \frac{4H_B}{\zeta_B}\{\mathbf{Q}'\mathbf{Q}'\}_B - \frac{4n'_B kT}{\zeta_B}\mathbf{I} - D_B \nabla'^2 \{\mathbf{Q}'\mathbf{Q}'\}_B = -c_B{}'\{\mathbf{Q}'\mathbf{Q}'\}_B n'_B + 2c_A{}'\{\mathbf{Q}'\mathbf{Q}'\}_A, \tag{6b}$$

where $(\cdot)_{(1')}$ represents the upper convected time derivative defined as

$$(\cdot) = \frac{D}{Dt'}(\cdot) - (\boldsymbol{\nabla}'\mathbf{v}')^{\intercal} \cdot (\cdot) - (\cdot) \cdot (\boldsymbol{\nabla}'\mathbf{v}').$$

Because the flow may be inhomogeneous, that is the number density of each species varies in space and time, $n'_\alpha(\mathbf{r}, t)$ can not be factored out of the second moment, that is

$$\{\mathbf{Q}'\mathbf{Q}'\}_\alpha \neq n'_\alpha < \mathbf{Q}'\mathbf{Q}' >_\alpha .$$

Finally, the total micellar contribution to the stress is given by

$$\boldsymbol{\sigma}' = H_A\{\mathbf{Q}'\mathbf{Q}'\}_A + H_B\{\mathbf{Q}'\mathbf{Q}'\}_B \tag{7}$$

2.1 Non-dimensionalization

The equations are nondimensionalized as follows:

$$\mathbf{r} = \frac{\mathbf{r}'}{d} \quad t = \frac{t'}{\lambda_{\text{eff}}} \quad \mathbf{v} = \frac{\lambda_{\text{eff}}\mathbf{v}'}{d} \quad \{\mathbf{QQ}\}_\alpha = \frac{H_A\{\mathbf{Q}'\mathbf{Q}'\}_\alpha}{n'^0_A kT} \quad n_\alpha = \frac{n'_\alpha}{n'^0_A}$$

where $\alpha = A,\ B$; d is a macroscopic characteristic length, in circular Couette geometry, $d = R_o - R_i$ where R_o, R_i are the outer and inner radii; λ_{eff} is the effective relaxation time of the network; and $\sqrt{n'^0_A kT/H_A}$ is a characteristic microscopic length scale for an elastic segment of species A where n'^0_A is the dimensional value of the number density of chains of length L at equilibrium conditions. The relaxation time of the α^{th} species is $\lambda_\alpha = \frac{\zeta_\alpha}{4H_\alpha}$. As opposed to being located solely at the beads, as in bead-spring dumbbells models, the drag is distributed along the chain, in accordance with network theory, and hence depends nonlinearly on the molecular weight of the chain.

As will be seen through fitting to experimental data, the shorter chains have a much shorter relaxation time, λ_B, than that of the longer chains, λ_A. Note that, since we only consider two species, we are tracking "all" short segments as species B and "all" long entangled chains as species A. Then, from reptation theory [33], one would expect that $\lambda_A \sim L^3/L_e$ where L_e is the entanglement length [6]. On the other hand, species B represents short segments with a Roussian-like relaxation, so that $\lambda_B \sim (L/2)^2$ [6]. These implies,

$$\frac{\lambda_A}{\lambda_B} \sim 4\frac{L}{L_e} >> 1, \tag{8}$$

hence, after the values of λ_A and λ_B are determined, the ratio in the right hand-side of Equation (8) should be an indicator of how long and/or entangled are the chains in the system. After we include more species, dependence on the molecular weight for the longer chains is expected to be $\lambda_\alpha \sim M_\alpha^{3.4}$ [34], [**?**].

We define,

$$\mathbf{A} = \int \mathbf{QQ}\Psi_A d\mathbf{Q} = \{\mathbf{QQ}\}_A, \tag{9a}$$

$$\mathbf{B} = \int \mathbf{QQ}\Psi_B d\mathbf{Q} = \{\mathbf{QQ}\}_B. \tag{9b}$$

Additionally, the dimesnionless breakage and reformation rates are given by

$$c_A = \lambda_A \, c'_A, \qquad c_B = \lambda_A \, n'^0_A \, c'_B \tag{10}$$

where c_A is the ratio of the relaxation time of the long chains to the breakage time of the long chain, similarly for c_B and the shorter chains. The ratio of the relaxation time of the short chains to the relaxation time of the long chains is denoted by,

$$\epsilon = \frac{\lambda_B}{\lambda_A}, \tag{11}$$

and that of the relaxation time of the long chains to the effective relaxation time of the network, as

$$\mu = \frac{\lambda_A}{\lambda_{\text{eff}}}. \tag{12}$$

The ratio of the spring constant of the shorter chains to that of the longer chains is

$$\frac{H_B}{H_A} \, = \, H^*. \tag{13}$$

If the network segments are ideal Hookean entropic springs, then we expect

$$H_B = \frac{3kT}{l^2 N_B} \qquad \text{and} \qquad H_A = \frac{3kT}{l^2 N_A} = \frac{3kT}{2l^2 N_B},$$

where N_α is the number of Kuhn steps of length l in the segment of species α. Note that $N_A = 2N_B$ so $H^* = 2$. The parameters ϵ, μ are to be determined by fitting to experiments.

Finally, the non-dimensional total stress $\boldsymbol{\sigma}$ is given by

$$\begin{aligned} \boldsymbol{\sigma} = \frac{\boldsymbol{\sigma}'}{G_0} &= (\{\mathbf{QQ}\}_A + H^* \{\mathbf{QQ}\}_B) \\ &= \mathbf{A} + 2\,\mathbf{B} \end{aligned} \tag{14}$$

where $G_0 = n'^0_A kT$.

2.2 Governing Equations

With the scaling and parameters introduced in Section 2.1, Equations (4)-(6) become

$$\mu\frac{Dn_A}{Dt} = 2\delta_A\nabla^2 n_A - \delta_A\nabla\nabla : \mathbf{A} + \frac{1}{2}c_B n_B^2 - c_A n_A, \tag{15a}$$

$$\mu\frac{Dn_B}{Dt} = 2\delta_B\nabla^2 n_B - 2\delta_B\ \nabla\nabla : \mathbf{B} - c_B n_B^2 + 2c_A n_A, \tag{15b}$$

$$\mu\mathbf{A}_{(1)} + \mathbf{A} - n_A\,\mathbf{I} - \delta_A\nabla^2\mathbf{A} = c_B\,n_B\,\mathbf{B} - c_A\mathbf{A}, \tag{16a}$$

$$\epsilon\mu\mathbf{B}_{(1)} + \mathbf{B} - \frac{n_B}{2}\,\mathbf{I} - \epsilon\delta_B\nabla^2\mathbf{B} = -2\epsilon\,c_B\,n_B\,\mathbf{B} + 2\epsilon\,c_A\mathbf{A}, \tag{16b}$$

Here we have defined non-dimensional diffusion constants $\delta_\alpha = \lambda_A D_\alpha/d^2$ for $\alpha = A, B$.

These equations for the number density and stress must be coupled with the fluid equations of conservation of mass, and of conservation of momentum:

$$\nabla\cdot\mathbf{v} = 0, \tag{17}$$

$$\mathrm{E}^{-1}\,\frac{\partial v}{\partial t} = \nabla\cdot\Pi, \tag{18}$$

where E is an elasticity number defined as

$$\mathrm{E} = \frac{G_0\lambda_{\mathrm{eff}}^2}{\rho d^2} = \frac{\mathrm{De}}{\mathrm{Re}}. \tag{19}$$

Here $\mathrm{Re} = \dfrac{\rho V' d}{\eta_0'}$ is the Reynolds number and $\mathrm{De} = \dfrac{\lambda_{\mathrm{eff}}V'}{d}$ is the Deborah number where V' is the velocity at the moving wall. Thus with our scaling the dimensionless value of the velocity at the moving boundary is De. The dimensionless diffusion constants are

$$\delta_A = \frac{\lambda_A D_A}{d^2} = \frac{\lambda_A V^{'}}{d}\ \cdot\ \frac{D_A}{V' d} = \frac{De}{Pe}$$

$$\delta_B = \frac{\zeta_A}{\zeta_B}\delta_A$$

where the Peclet number is $V^{'}d/D_A$ and is a measure of relative importance of convection to diffusion of the elastic chains of species A.

In addition, the total stress tensor is given by

$$\Pi = p\mathbf{I} - \beta\dot{\boldsymbol{\gamma}} + \boldsymbol{\tau}, \tag{20}$$

where the extra stress arising from the network is

$$\boldsymbol{\tau} = (n_A + n_B)\mathbf{I} - (\mathbf{A} + 2\mathbf{B}), \tag{21}$$

and $\beta = \dfrac{\eta_s}{\eta_0{}'}$, where η_s is the solvent viscosity, and $\eta_0{}'$ is the dimensional zero shear rate viscosity.

To solve the system of equations (17) - (20), appropriate boundary and initial conditions on both stress and velocity need to be specified. In this paper spatial variations are not considered, thus boundary conditions are not required at this point. A full discussion of boundary conditions will be given in Part III [28], where the full inhomogeneous flow is solved numerically.

On the other hand, initial values are found from Equations (15)-(16) assuming equilibrium conditions. That is, in absence of flow, $n_A^0 = 1$ and Equation (15a) gives

$$n_B^0 = \sqrt{\frac{2c_{A\text{eq}}}{c_{B\text{eq}}}}, \tag{22}$$

where $c_{A\text{eq}}, c_{B\text{eq}}$ are the values of the breakage and reformation rates c_A, c_B at equilibrium.

Similarly, at equilibrium we obtain

$$\begin{aligned} \mathbf{A}_{\text{eq}} &= \mathbf{I}, \\ \mathbf{B}_{\text{eq}} &= \frac{n_B^0}{2}\mathbf{I} \end{aligned}$$

2.3 Determination of Breakage Rate

So far we have developed a general two species network model for the evolution of stess and number density of elastic segments of length Q_A, Q_B. To complete the model we need to specify appropriate breakage and reformation rates that describe the evolution of the number density of each species under both equilibrium and flowing conditions. In principle appropriate expressions could be determined by Brownian dynamics calculations of entangled wormlike micelles in the same manner as the studies of van den Brule *et. al.* [18] and Hernandez-Cifre *et. al.* [16] for associative polymer networks. However, such simulations are complicated by the multiple breaking and reforming events expected for each chain. In the present work we thus

use simplified analytic expressions for each term. In particular, the dependence of the breakage rate on the flow strength is taken as a term consistent with the partial retraction term as proposed by Larson [35]. In this work Larson considered the dynamics of network segments which are convected by a flow but which do not deform affinely inside their bounding tubes. The resulting partially-extending convected (PEC) strand model provides a simple differential analog of Doi-Edwards reptation theory. The longer elastic segments, species A, in our model will experience similar convection by the flow and partial retraction following a breakage event before being reincorporated into the network. We thus write

$$c_A = c_{A\,\mathrm{eq}} + \frac{1}{3}\,\xi\mu\left(\dot{\boldsymbol{\gamma}} : \frac{\mathbf{A}}{n_A}\right), \tag{23a}$$

$$c_B = c_{B\,\mathrm{eq}}. \tag{23b}$$

A term with similar functional form to that in our breaking term is used in the single species differential model of Marrucci *et. al.* [36] and in Likhtman and Graham's non-extendable limit of their Rolie-Poly model [37]. Although in the latter two cases full retraction of the molecule within the tube is assumed, in the analogue to the Larson's form the parameter ξ is allowed to vary from 0 to 1 to capture the partial retraction of a polymer within a tube constraint. When $\xi = 0$ this corresponds to no retraction or ideal affine neo-Hookean behavior, the resulting constitutive equation is of simple convected Maxwell form [30]. When $0 < \xi < 1$ this corresponds to partial extension and retraction. Finally, when $\xi = 3/5$ this corresponds to full retraction of the chain segment inside the deforming tube, or Doi-Edwards theory.

Larson's term, which represents tube breakage after partial retraction, is used in our case to model micelle breakage. We have introduced this term as an explicit breakage term in our two species model as opposed to as a non-affine derivative in a single species model, as introduced by Larson. Thus the nonaffineness of the motion arises due to the breaking and the reforming.

The advantage of the Larson-type term, in the single species case, is that it not only predicts a shear banding situation -provided a solvent viscosity is added to the model similar to the Johnson-Segalman model- but that also, unlike the Johnson-Segalman model, it obeys the Lodge-Meissner relation in step strain and it exhibits a maximum in elongational viscosity as a function of elongation rate [25]. Larson's single species model has shown good agreement with shear, extensional, and step strain experimental data of certain

polymers, although it was noted that different values of the parameter ξ are needed for each type of deformation [25], [38].

A similar expression to the one in Equation (23a), is also used in the two species network model of Tripathi *et. al.* [19] for associative polymer networks to describe the creation rate of bridging chains from dangling chains. The difference between that model and the model presented here is that our model incorporates inhomogeneities in the flow, and that Tripathi *et. al.* explicitly modeled the molecular weight effect of the breaking rate of the bridging chains, which we have not included. In addition, the creation and destruction of each species is modeled as a first order reaction in the Tripathi case, where the creation of long chains is quadratic in our model as it inherently involves the combination of two shorter chains rather than the reincorporation of a dangling chain into an elastic network.

3 Viscometric Predictions in Homogeneous Flow

Experiments with wormlike micellar solutions carried out in cylindrical Couette devices show that spatial variations develop in the flow above a critical shear rate [8] [10], [39], [40], [41]. In the formulation of the present model diffusion terms are included in order to capture the observed physical inhomogeneities such as shear banding. However, to understand the underlying viscometric behavior we first consider Equations (15)-(16) in the absence of spatial variation, thus we assume $\delta_A = \delta_B = 0$ and $\dot{\boldsymbol{\gamma}}(\mathbf{r})$ constant. Here we present the formulation and rheological predictions of this two species model under such assumptions.

3.1 Shear Flow in Circular - Couette Geometry

We employ the following assumptions of a homogeneous unidirectional shear flow,

$$\begin{aligned}
\mathbf{v} &= (0, v(r), 0) \\
\mathbf{v} \cdot \nabla(\cdot) &= 0 \\
\dot{\boldsymbol{\gamma}} &= \dot{\gamma}_0 \, \boldsymbol{\delta}_r \boldsymbol{\delta}_\theta + \dot{\gamma}_0 \, \boldsymbol{\delta}_\theta \boldsymbol{\delta}_r \\
\dot{\gamma}_0 &= r \frac{\partial}{\partial r} \left(\frac{v}{r} \right) \\
\dot{\boldsymbol{\gamma}} : \mathbf{A} &= 2 \, \dot{\gamma}_0 \, A_{r\theta},
\end{aligned}$$

and equations (15)-(16) to find evolution equations for the number densities and stress contributions, from species A and B, as functions of $\dot{\gamma}_0$. We thus obtain the following expressions for number density's of each species:

$$\mu \frac{dn_A}{dt} = \frac{1}{2} c_{B\,\mathrm{eq}}\, n_B^2 - \frac{2}{3}\,\xi\,\mu\dot{\gamma}_0\, A_{r\theta} - c_{A\,\mathrm{eq}}\, n_A \tag{24a}$$

$$\mu \frac{dn_B}{dt} = -c_{B\,\mathrm{eq}}\, n_B^2 + \frac{4}{3}\,\xi\,\mu\dot{\gamma}_0\, A_{r\theta} + 2\, c_{A\,\mathrm{eq}}\, n_A \tag{24b}$$

and for the components of the stress tensor $\mathbf{A}$ for species A:

$$\mu \frac{dA_{rr}}{dt} + A_{rr} - n_A = c_{B\,\mathrm{eq}}\, n_B\, B_{rr} - \frac{2}{3}\,\xi\,\mu\dot{\gamma}_0\, \frac{A_{r\theta}}{n_A} A_{rr} - c_{A\,\mathrm{eq}}\, A_{rr} \tag{25a}$$

$$\mu \frac{dA_{r\theta}}{dt} - \mu\dot{\gamma}_0\, A_{rr} + A_{r\theta} = c_{B\,\mathrm{eq}}\, n_B\, B_{r\theta} - \frac{2}{3}\,\xi\,\mu\dot{\gamma}_0\, \frac{A_{r\theta}}{n_A} A_{r\theta} - c_{A\,\mathrm{eq}}\, A_{r\theta} \tag{25b}$$

$$\mu \frac{dA_{\theta\theta}}{dt} - 2\,\mu\dot{\gamma}_0\, A_{r\theta} + A_{\theta\theta} - n_A = c_{B\,\mathrm{eq}}\, n_B\, B_{\theta\theta} - \frac{2}{3}\,\xi\,\mu\dot{\gamma}_0\, \frac{A_{r\theta}}{n_A} A_{\theta\theta} - c_{A\,\mathrm{eq}}\, A_{\theta\theta} \tag{25c}$$

$$\mu \frac{dA_{zz}}{dt} + A_{zz} - n_A = c_{B\,\mathrm{eq}}\, n_B\, B_{zz} - \frac{2}{3}\,\xi\,\mu\dot{\gamma}_0\, \frac{A_{r\theta}}{n_A} A_{zz} - c_{A\,\mathrm{eq}}\, A_{zz} \tag{25d}$$

and finally for the stress associated with species B:

$$\epsilon\mu\frac{dB_{rr}}{dt} + B_{rr} \;-\; \frac{1}{2}\,n_B = \epsilon\left[-2c_{B\,\mathrm{eq}}\,n_B\,B_{rr} + \frac{4}{3}\,\xi\,\mu\dot{\gamma}_0\,\frac{A_{r\theta}}{n_A}A_{rr} \;+\; 2\,c_{A\,\mathrm{eq}}\,A_{rr}\right] \tag{26a}$$

$$\epsilon\mu\frac{dB_{r\theta}}{dt} - \epsilon\mu\dot{\gamma}_0\,B_{rr} \;+\; B_{r\theta} = \epsilon\left[-2c_{B\,\mathrm{eq}}\,n_B\,B_{r\theta} + \frac{4}{3}\,\xi\,\mu\dot{\gamma}_0\,\frac{A_{r\theta}}{n_A}A_{r\theta} \;+\; 2\,c_{A\,\mathrm{eq}}\,A_{r\theta}\right] \tag{26b}$$

$$\epsilon\mu\frac{dB_{\theta\theta}}{dt} - 2\,\epsilon\mu\dot{\gamma}_0\,B_{r\theta} \;+\; B_{\theta\theta} \;-\; \frac{1}{2}\,n_B = \epsilon\left[-2c_{B\,\mathrm{eq}}\,n_B\,B_{\theta\theta} + \frac{4}{3}\,\xi\,\mu\dot{\gamma}_0\,\frac{A_{r\theta}}{n_A}A_{\theta\theta} \;+\; 2\,c_{A\,\mathrm{eq}}\,A_{\theta\theta}\right] \tag{26c}$$

$$\epsilon\mu\frac{dB_{zz}}{dt} + B_{zz} \;-\; \frac{1}{2}\,n_B = \epsilon\left[-2c_{B\,\mathrm{eq}}\,n_B B_{zz} + \frac{4}{3}\,\xi\,\mu\dot{\gamma}_0\,\frac{A_{r\theta}}{n_A}A_{zz} \;+\; 2\,c_{A\,\mathrm{eq}}\,A_{zz}\right] \tag{26d}$$

3.2 Extensional Flow

For homogeneous uniaxial extensional flow with extension rate $\dot{\varepsilon}_0$ we have:

$$\begin{aligned}
\mathbf{v} &= \left(-\frac{1}{2}\dot{\varepsilon}_0\,r, 0, \dot{\varepsilon}_0\,z\right)\\
\mathbf{v}\cdot\nabla(\cdot) &= 0\\
\dot{\boldsymbol{\gamma}} &= -\,\dot{\varepsilon}_0\,\boldsymbol{\delta}_r\boldsymbol{\delta}_r \;-\; \dot{\varepsilon}_0\,\boldsymbol{\delta}_\theta\boldsymbol{\delta}_\theta \;+\; 2\,\dot{\varepsilon}_0\,\boldsymbol{\delta}_z\boldsymbol{\delta}_z\\
\dot{\boldsymbol{\gamma}} : \mathbf{A} &= \dot{\varepsilon}_0\;(2A_{zz} \;-\; A_{rr} \;-\; A_{\theta\theta}) = 2\,\dot{\varepsilon}_0\,(A_{zz} - A_{rr})
\end{aligned}$$

Equations (15)-(16) give for the number densities of species A and B:

$$\mu\frac{dn_A}{dt} = \frac{1}{2}\,c_{B\,\mathrm{eq}}\,n_B^2 \;-\; \frac{2}{3}\,\xi\,\mu\dot{\varepsilon}_0\;(A_{zz} \;-\; A_{rr}) \;-\; c_{A\,\mathrm{eq}}\,n_A \tag{27a}$$

$$\mu\frac{dn_B}{dt} = -c_{B\,\mathrm{eq}}\,n_B^2 + \frac{4}{3}\,\xi\,\mu\dot{\varepsilon}_0\;(A_{zz} \;-\; A_{rr}) \;+\; 2\,c_{A\,\mathrm{eq}}\,n_A \tag{27b}$$

and for the components of the stress tensor $\mathbf{A}$ for species A:

$$\mu\frac{dA_{rr}}{dt}+\mu\dot{\varepsilon}_0\,A_{rr}\;+\;A_{rr}\;-\;n_A= c_{B\,\mathrm{eq}}\,n_B\,B_{rr}\;-\frac{2}{3}\,\frac{\xi\,\mu\dot{\varepsilon}_0}{n_A}\;(A_{zz}-A_{rr})\;A_{rr}\;-\;c_{A\,\mathrm{eq}}\,A_{rr} \tag{28a}$$

$$\mu\frac{dA_{r\theta}}{dt}+A_{r\theta}= c_{B\,\mathrm{eq}}\,n_B\,B_{r\theta}\;-\frac{2}{3}\,\frac{\xi\,\mu\dot{\varepsilon}_0}{n_A}\;(A_{zz}-A_{rr})\;A_{r\theta}\;-\;c_{A\,\mathrm{eq}}\,A_{r\theta} \tag{28b}$$

$$\mu\frac{dA_{zz}}{dt}-2\,\mu\dot{\varepsilon}_0\,A_{zz}\;+\;A_{zz}\;-\;n_A= c_{B\,\mathrm{eq}}\,n_B\,B_{zz}-\frac{2}{3}\,\frac{\xi\,\mu\dot{\varepsilon}_0}{n_A}\;(A_{zz}-A_{rr})\;A_{zz}\;-\;c_{A\,\mathrm{eq}}\,A_{zz} \tag{28c}$$

and finally for the stress associated with species B:

$$\epsilon\mu\frac{dB_{rr}}{dt}+\epsilon\mu\dot{\varepsilon}_0\,B_{rr}\;+\;B_{rr}\;-\;\frac{1}{2}\,n_B=\epsilon\Bigg[-2c_{B\,\mathrm{eq}}\,n_B\,B_{rr}+\frac{4}{3}\,\frac{\xi\,\mu\dot{\varepsilon}_0}{n_A}\;(A_{zz}-A_{rr})\;A_{rr}\;+2c_{A\,\mathrm{eq}}\,A_{rr}\Bigg] \tag{29a}$$

$$\epsilon\mu\frac{dB_{r\theta}}{dt}\;+\;B_{r\theta}=\epsilon\Bigg[-2c_{B\,\mathrm{eq}}\,n_B\,B_{r\theta}+\frac{4}{3}\,\frac{\xi\,\mu\dot{\varepsilon}_0}{n_A}\;(A_{zz}-A_{rr})\;A_{r\theta}\;+2c_{A\,\mathrm{eq}}\,A_{r\theta}\Bigg] \tag{29b}$$

$$\epsilon\mu\frac{dB_{zz}}{dt}\;-\;2\,\epsilon\mu\dot{\varepsilon}_0\,B_{zz}+\;B_{zz}\;-\;\frac{1}{2}\,n_B=\epsilon\Bigg[-2c_{B\,\mathrm{eq}}\,n_B\,B_{zz}+\frac{4}{3}\,\frac{\xi\,\mu\dot{\varepsilon}_0}{n_A}\;(A_{zz}-A_{rr})\;A_{zz}\;+2c_{A\,\mathrm{eq}}\,A_{zz}\Bigg] \tag{29c}$$

The equations for $A_{\theta\theta}$ and $B_{\theta\theta}$ are identical to those for A_{rr}, B_{rr} respectively with all rr components changes to $\theta\theta$ components. Note that if $A_{r\theta}, B_{r\theta}$ are initiatily zero, they stay identically zero. Hence this component of the stress does not play an important role in extensional flow except in preshear conditions such that $A_{r\theta}, B_{r\theta}$ are not zero at the start of the extensional flow.

4 Linear Viscoelasticity

We now proceed to solve the constitutive equations to evaluate the steady and transient rheological predictions. We first consider the linearized limit

of small deformations. In general, as will be seen below, fitting the linearized equations in shear to linear viscoelastic data only serves to determine $\lambda_{\rm eff} = \lambda_A/(1 + c_{A\,\rm eq})$ and $\lambda_2 n_B^0 = \lambda_2\sqrt{2c_{A\,\rm eq}/c_{B\,\rm eq}}$. In order to fully determine the appropriate parameters, in particular the magnitude of $c_{A\,\rm eq}$ and $c_{B\,\rm eq}$, nonlinear deformations must be considered such as step strain, steps in shear, and extension flows.

4.1 Small Amplitude Oscillatory Cylindrical Shear Flow (SAOS).

In this section we develop linear theory in SAOS flow. Assuming that

$$\gamma_{r\theta} = \Re{\rm e}\{\gamma^0 \exp^{i\omega t}\} \quad \text{and} \quad \gamma^0 << 1,$$

where $\omega = \lambda_{\rm eff}\omega'$ is the dimensionless oscillation frequency. Inserting this into Equations (24)-(26), and keeping only linear terms in γ^0 we obtain

$$i\mu\omega A^1_{r\theta} + (1 + c_{A\rm eq})A^1_{r\theta} - c_{B\,\rm eq}n^0_B B^1_{r\theta} = i\mu\omega\gamma^0 A^0_{rr} \tag{30a}$$

$$(1 + c_{A\rm eq})A^0_{rr} - c_{B\,\rm eq}n^0_B B^0_{rr} = n^0_A = 1 \tag{30b}$$

$$i\epsilon\mu\omega B^1_{r\theta} + B^1_{r\theta}(1 + 2\epsilon c_B n_B) - 2c_{A\rm eq}\epsilon A^1_{r\theta} = i\epsilon\mu\omega\gamma^0 B^0_{rr} \tag{30c}$$

$$B^0_{rr}(1 + 2\epsilon c_{B\,\rm eq}n^0_B) = \frac{1}{2}n^0_B + 2\epsilon c_{A\rm eq}A^0_{rr} \tag{30d}$$

$$c_{B\,\rm eq}\, n_B^2 - 2\, c_{A\rm eq} = 0 \tag{30e}$$

Note that in linearized small disturbance theory the number density of each species, n^0_A and n^0_B, are constant since variations in these terms are introduced in the full equations (24) by quadratically small terms. In these linearized equations all quantities are nondimensional as before. Equations (30b) and (30d) give, after ignoring $O(\epsilon)$ terms,

$$B^0_{rr} = \frac{1}{2}n^0_B, \tag{31a}$$

$$A^0_{rr} = 1. \tag{31b}$$

Thus, for ϵ small and $c_{A\rm eq}$, $c_{B\,\rm eq} = {\rm O}(1)$ in ϵ, we have

$$A^0_{rr} = 1, \tag{32a}$$

$$B^0_{rr} = \frac{1}{2}n^0_B, \tag{32b}$$

$$A^1_{r\theta} = \gamma^0\left(\frac{\left(\frac{\mu}{1+c_{A\rm eq}}\,\omega\right)^2}{1 + \left(\frac{\mu}{1+c_{A\rm eq}}\,\omega\right)^2} + \frac{i\frac{\mu}{1+c_{A\rm eq}}\,\omega}{1 + \left(\frac{\mu}{1+c_{A\rm eq}}\,\omega\right)^2}\right) + ..., \tag{32c}$$

$$B^1_{r\theta} = \gamma^0\frac{n^0_B}{2}\left(\frac{(\epsilon\mu\omega)^2}{1 + (\epsilon\mu\omega)^2} + \frac{i\epsilon\mu\omega}{1 + (\epsilon\mu\omega)^2}\right) + ... \tag{32d}$$

In the limit of small frequencies the system behaves as a single mode Maxwellian system. Our system of equations has been nondimensionalized by this mode's effective time and hence we use Equation (32c) to define the effective relaxation time, λ_{eff}, as

$$\lambda_{\text{eff}} = \frac{\lambda_A}{1 + c_{A\text{eq}}} = \frac{\lambda_A}{1 + \lambda_A c'_{A\text{eq}}} = \frac{1}{\frac{1}{\lambda_A} + c'_{A\text{eq}}}, \tag{33}$$

which results from $\mu/(1 + c_{A\text{eq}}) = 1$ and, λ_{eff} has units of seconds.

Equation (33) shows that the overall relaxation time of the network, λ_{eff}, is reduced from the longest relaxation time of the elastic chains, λ_A, due to the additional mechanism of breakage. Thus, the stress relaxes either through chains of length L relaxing or through the chains of length L breaking to form chains of length $L/2$. This scaling of the effective relaxation time is a result of the simplification of the continuous Cates' breaking dynamics to a two species discrete limit. Recall that in the continuous limit Cates showed that $\lambda_{\text{eff}} = (\lambda_A \lambda_{\text{break}})^{\frac{1}{2}}$. Finally, for all values of ω the linear system behaves as the superposition of two Maxwell modes with relaxation times λ_{eff} and λ_B respectively.

From these results the zero shear rate viscosity is given, to order ϵ, by

$$\eta_0{}' \quad = \quad n_A'^0 kT \frac{\lambda_A}{1 + \lambda_A c'_{1\text{eq}}} = G_0 \lambda_{\text{eff}}.$$

For a fixed relaxation time of the longer species, λ_A, the dimensional zero shear rate viscosity of the mixture decreases as the breaking rate at equilibrium, $c'_{A\text{eq}}$, increases. That is, the effective relaxation time decreases as the breakage rate increases. Figure 2a shows η'_0 as a function of the breakage rate $c'_{A\text{eq}}$, for different values of λ_A. In Figure 2b, $c'_{A\text{eq}}$ is kept fixed at different values, and η'_0 is plotted against λ_A. Experiments have shown that for a given solution the zero shear rate viscosity increases nonlinearly with increasing surfactant concentration [42], [43], [9]. Hence in our model, $c'_{A\text{eq}}$ and λ_A play an important role in determining the effect of concentration and salinity. That is, in order to change $c'_{A\text{eq}}$ or λ_A one would need to change the concentration of polymer, the concentration of salt, and/or change the type of salt counterion.

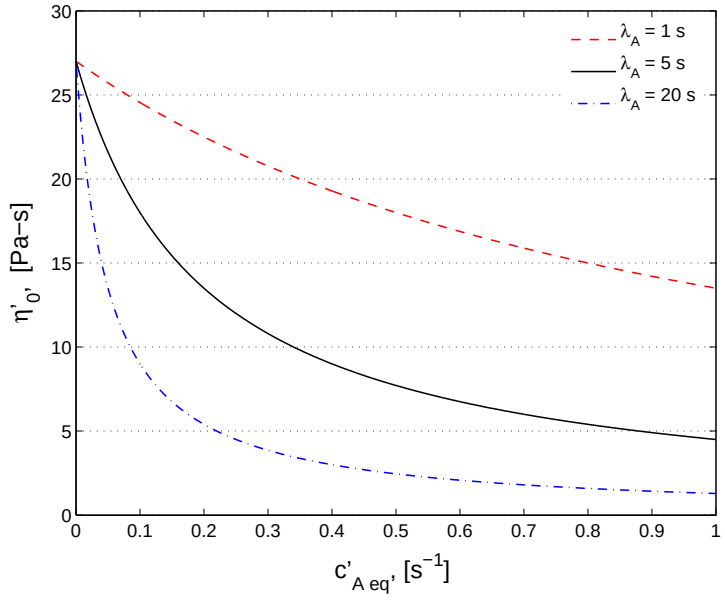

(a)

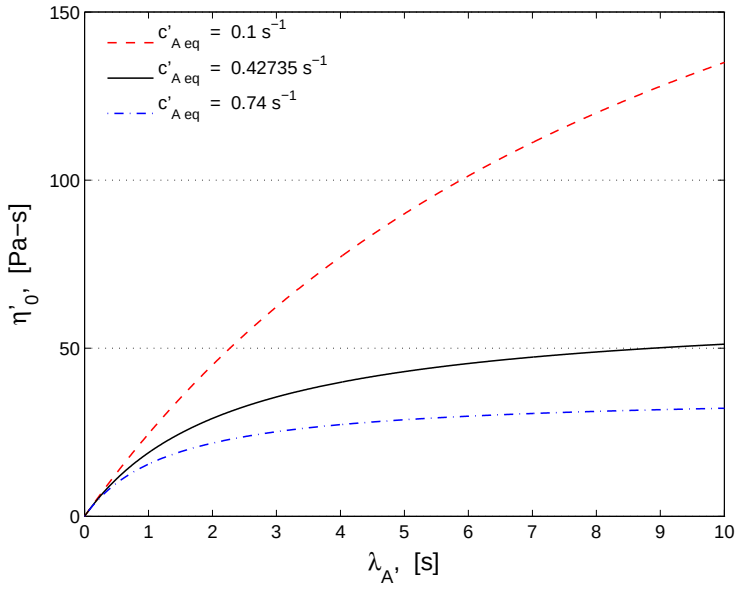

(b)

Figure 2: Variations on the zero shear rate viscosity for: (a) different relaxation times of species A, λ_A, and (b) different breaking rates at equilibrium, $c'_{1\text{eq}}$. In these figures, $G_0 = 27$ Pa.

5 Evaluation of Model Parameters

The characteristic stress scale for the micellar network is given by $G_0 = n_A^{\prime 0} kT$. Following this nondimensionalization, the response of a particular micellar solution to nonlinear deformations is described in this model by three independent parameters. At first glance, the model appears to contain six parameters: λ_A, λ_B, $c_{A\mathrm{eq}}$, $c_{B\mathrm{eq}}$, n_B^0, and ξ. However, five of the parameters are related to one another through three independent equations. In the first of these we see from (15a) that the reaction rates $c_{A\mathrm{eq}}$, $c_{B\mathrm{eq}}$, and the number density of the second species n_B^0 are related by

$$n_B^0 = \sqrt{\frac{2c_{A\mathrm{eq}}}{c_{B\mathrm{eq}}}}.$$

Recall that the number densities were nondimensionalized by $n_A^{0\prime}$ so that $n_A^0 = 1$. Similarly, when the effective relaxation time of the solution, λ_{eff}, is known, a relation between λ_A and $c'_{A\mathrm{eq}}$ is established by means of Equation (33). Finally, in the linear viscoelastic regime the model reduces to a two mode Maxwell model and the amplitude of the second mode is governed by the product

$$\lambda_B n_B^0 = \text{constant},$$

where the constant is found by fitting to experiments and determines a relation between n_B^0 and λ_B.

Consequently, there are only three parameters to be determined for a given micellar mixture. One of these is the slippage parameter ξ, which only appears in non-linear flows, and which determines the magnitude of the contribution from the stress/strain rate dependent term to the breaking rate. The other two parameters to be fitted can be chosen arbitrary from the remaining five. In this study we have chosen these two parameters to be n_B^0 and $c'_{A\mathrm{eq}}$.

From Equations (32c)-(32d) the storage and loss modulus are given by

$$G' = G_0 \left\{ \frac{(\lambda_{\mathrm{eff}}\omega')^2}{1+(\lambda_{\mathrm{eff}}\omega')^2} + n_B^0 \frac{(\lambda_B\omega')^2}{1+(\lambda_B\omega')^2} \right\} \tag{34a}$$

$$G'' = G_0 \left\{ \frac{\lambda_{\mathrm{eff}}\omega'}{1+(\lambda_{\mathrm{eff}}\omega')^2} + n_B^0 \frac{\lambda_B\omega'}{1+(\lambda_B\omega')^2} \right\} \tag{34b}$$

In the linear viscoelastic regime provided λ_{eff} and $\lambda_B n_B^0$ are kept constant, the plot of the storage and loss modulus versus frequency remains the

same, as is shown in Figure 3. Fitting of these curves as predicted by the model with experimental data [9] are shown there. Figure 4 shows the effect of changing these parameters. That is, Figure 4a shows the effect of decreasing the effective relaxation time, by either increasing $c'_{A\text{eq}}$ or decreasing λ_A according to

$$\frac{1}{\lambda_{\text{eff}}} = \frac{1}{\lambda_A} + c'_{A\text{eq}},$$

and Figure 4b shows that if either n_B^0 or λ_B is increased, the contribution from the second mode increases.

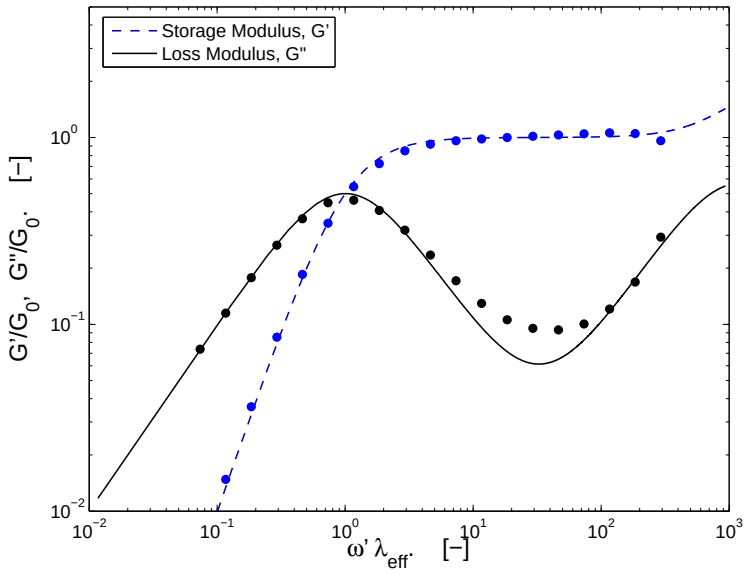

Figure 3: Non-dimensional storage and loss modulus model prediction compared with experimental data from a solution of 100 mM CpyCl [9]. In this figure $\lambda_B n_B^0 = 1 \times 10^{-3}$ sec., $\lambda_{\text{eff}} = 1.17$ sec., and $G_0 = 27$ Pa.

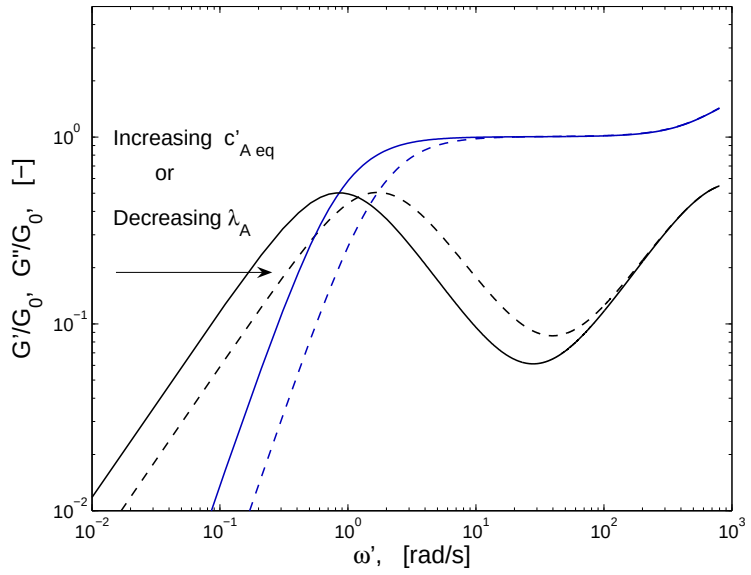

(a)

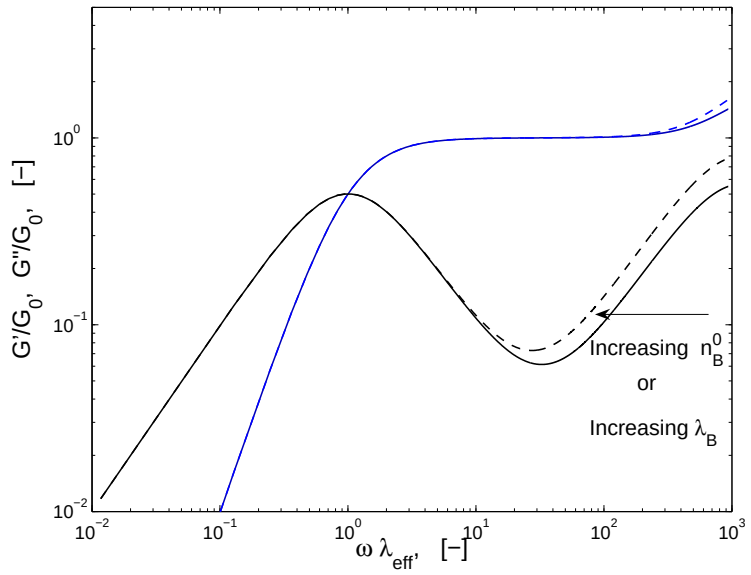

(b)

Figure 4: Variations in the predicted loss and storage moduli: (a) Effect of decreasing λ_{eff} by either increasing the breaking rate $c'_{A\text{eq}}$ or decreasing the micellar relaxation time λ_A; (b) Effect of increasing the number density of species B, n_B^0, or λ_B. Here the solid line corresponds to the parameters in Figure 3, the dashed line is the result arising from the variation of the indicated parameter. Other parameter values are kept as in Figure 3.

Next we examine the model predictions under three different nonlinear deformations: step strain, steady state shear flow, and steady state uniaxial elongational flow. First we discuss some general considerations and asymptotic behavior of the model for these deformation histories. This is followed by exploration of model predictions under these deformation histories as the parameters $c'_{A\text{eq}}$, n_B^0, and ξ are varied.

5.1 Step Strain Calculations

Because the evolution equations for number density and stress are strongly coupled, it is necessary to integrate them in the beginning from equilibrium conditions. To simulate step strain experiments, Equations (24) - (26), were integrated in time with an imposed strain given by

$$\gamma'(t') = \gamma'_0 \left(1 - \left(1 + at'\right) \exp(-bt')\right). \tag{35}$$

where the parameters a and b were fitted to the experimental motor response [13]. For large b this is the achievable experimental approximation to a Heaviside function in time. For the curves presented in this paper we have taken $b = 64.4$ s^{-1} and $a = 143.6$ s^{-1}.

Results for the stress relaxation as a function of time for different applied strains are shown in Figure 5. In the insert the results are graphed with the y-axis on logarithmic scale and the x-axis on a linear scale. It can be seen, in the insert, that for every value of γ_0 the slope of each of the parallel lines, after the initial transient is completed, is -1. This indicates that the stress can be factored as

$$\sigma'_{r\theta}(\gamma, t) = \gamma\, G_0\, g(t)\, h(\gamma) = \gamma\, G(t)\, h(\gamma) \tag{36}$$

where

$$G(t) = G_0 \exp(-t) = G_0 \exp\left(-\frac{t'}{\lambda_{\text{eff}}}\right) \tag{37}$$

Thus, if the stress is scaled by a factor $\gamma_0 h(\gamma_0)$ all the curves will superpose. This behavior remains unchanged as long as λ_{eff} and $\lambda_B n_B^0$ are kept constant.

Analytic considerations show that the model predicts

$$h(\gamma) = e^{-\xi\gamma^2/3} + O(\epsilon\mu b). \tag{38}$$

If $c_{A\text{eq}} \sim c_{B\text{eq}} \sim 0$, and $\epsilon\mu b << 1$ then to a good approximation

$$h(\gamma) = e^{-\xi\gamma^2/3}. \tag{39}$$

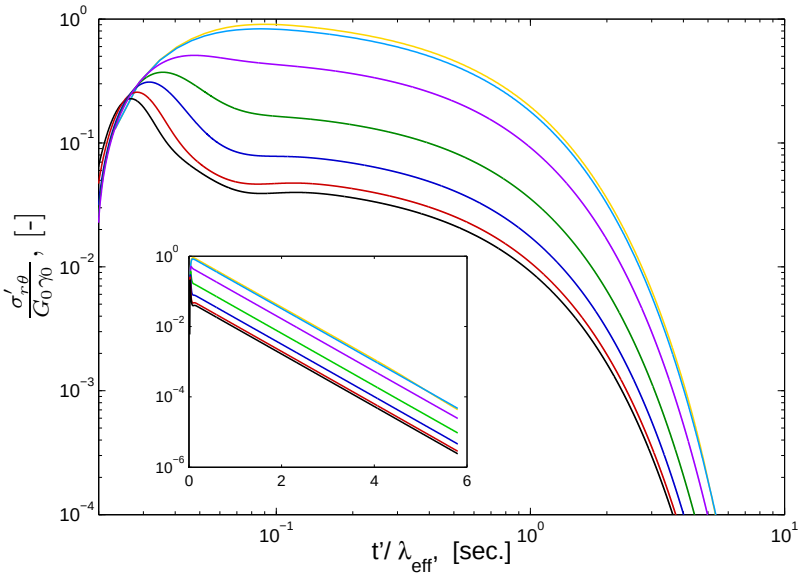

Figure 5: Model predictions of stress relaxation after sudden deformation for $\gamma_0 = 0.1$, 1, 3, 5, 7, 10, 12. Insert: Stress relaxation in linear-log scale. In this figure $\xi = 0.3$ and $\epsilon = 6.5 \times 10^{-5}$.

When $c_{A\text{eq}}, c_{B\text{eq}} >> 1$, terms of order $\epsilon\mu b$ are no longer negligible and they have an effect on the behavior of $h(\gamma)$. The numerical best fit for the damping function suggests

$$h(\gamma) = \frac{1}{1 + 0.3\,(\sqrt{\xi}\gamma)^3} \tag{40}$$

as shown in Figure 7a.

5.2 Homogeneous Shear Flow

Equations (24) - (26) were integrated numerically in time to steady state subject to a constant dimensionless shear rate $\dot{\gamma}_0 = (\lambda_{\text{eff}}\dot{\gamma}'_0)$. Figure 6 shows plots of the steady state shear stress and the first normal stress difference as functions of shear rate. The resulting flow curves are nonmonotonic. Beyond a critical deformation rage, $\dot{\gamma}'_1$, the scission of A network strands overwhelms the increased stretching that arises from increasing shear. At very high deformation rates the growth in the stress is again linear with respect to the shear rate. A possible behavior unde inhomogeneous conditions, which permit the formation of shear bands, is shown in dashed lines. Recall that

$$\sigma_{r\theta} = A_{r\theta} + 2\, B_{r\theta}.$$

From (24) - (26) it can be seen that for $\dot{\gamma_0} << 1$, $B_{r\theta} \sim 0$ and

$$\sigma_{r\theta} \sim A_{r\theta} \sim \dot{\gamma}_0.$$

On the other hand, at large shear rates, $\dot{\gamma_0} >> 1$, most of the chains of length L have been destroyed, hence the flow response is dominated by the short species which in this limit give rise to a stress of

$$B_{r\theta} \sim \left(1 + \frac{n_B^0}{2}\right) \mu\, \epsilon\, \dot{\gamma}_0,$$

so that:

$$\sigma_{r\theta} \sim 2\, B_{r\theta} \sim \frac{\lambda_B(2 + n_B^0)}{\lambda_{\text{eff}}}\, \dot{\gamma}_0.$$

The non-monotonic behavior at the intermediate rates, where contributions from both species vary due to breaking and reforming mechanisms, can be resolved only by performing inhomogeneous flow calculations in which a plateau is allowed to develop in the the stress/shear rate curve and shear bands are formed by the selection of different local shear rates. Calculations with other nonlocal constitutive models show that the precise shape of these curves depends on the dimensionless diffusivities, δ_A, δ_B, the flow loading history and the geometry [20]. In the present study we do not consider spatial variations. As a consequence the formation of such a plateau, the radial positions, and the slopes of the shear bands are not studied here; our efforts in analyzing the non-homogeneous case will be presented in a subsequent study [28].

Additionally the model predicts, under homogeneous flow conditions, that the maximum in the shear stress is given by

$$(\dot{\gamma}_0\,\lambda_{\text{eff}})_{max} = f(c_{1\text{eq}}, c_{2\text{eq}})\sqrt{\frac{1}{\xi}} \tag{41a}$$

$$\left(\frac{\sigma_{r\theta}}{G_0}\right)_{max} = \frac{g(c_{1\text{eq}}, c_{2\text{eq}})}{\xi\dot{\gamma}_0} = \frac{g(c_{1\text{eq}}, c_{2\text{eq}})}{f(c_{1\text{eq}}, c_{2\text{eq}})}\sqrt{\frac{1}{\xi}}. \tag{41b}$$

However, in inhomogenous flow conditions, the plateau it is not realized by "top jumping" and hence such plateau is expected to be at a value less than one [28]. Furthermore, as point out by Berret *et. al.* [44], the non-dimensional values in Equation (41) are highly dependent on the surfactant concentration. Then, in our model, such a dependence will be on the parameters $c_{1\text{eq}}$, $c_{2\text{eq}}$, and n_B^0.

The first normal stress difference grows quadratically in the limit of small deformation rates and asymptotically approaches the limit $2G^{'}\dot{\gamma}^2$ as $\dot{\gamma}$ goes to zero as expected from simple fluid theory. The homogeneous solution exhibits a nonmonotonicity similar to that observed in the shear stress at intermediate rates before increasing quadratically again at high rates due to the contribution of the short elastic B species. On the other hands, inspection of Equations (15)-(16) shows that $N_2 = \sigma_{rr} - \sigma_{zz} = 0$.

Although the precise form of the elastic first normal stress difference in the inhomogeneous shear-banding region can not be determined without solving the full inhomogeneous equation set, we anticipate a change of slope but not a plateau, due to the coupling between the shear stress and the velocity field, which, at least in the case of no scission/reformation, gives rise to terms of the form $2\lambda_{\text{eff}}\sigma_{r\theta}(\dot{\gamma})\dot{\gamma} \sim \dot{\gamma}$ in the region where $\sigma_{r\theta}$ is constant, that is plateaus, that is in the shear banding region.

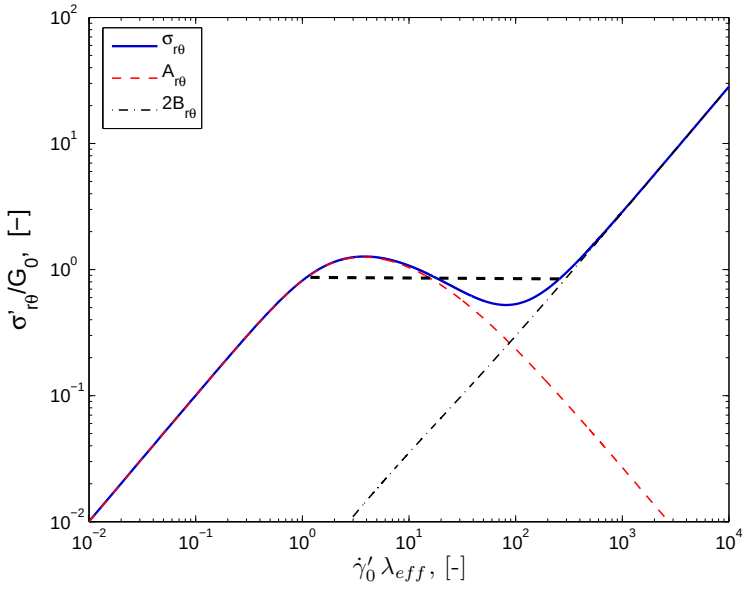

(a)

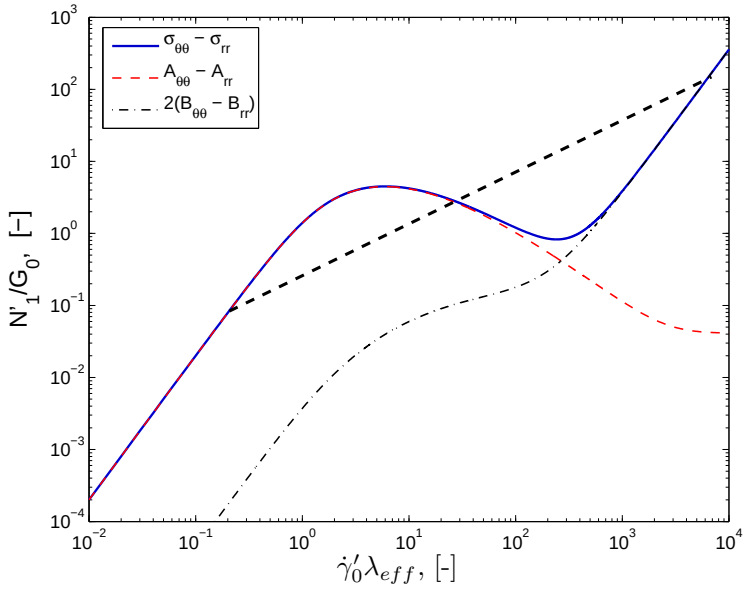

(b)

Figure 6: Model predictions in steady state shear flow as a function of $\dot{\gamma}_0$. Here $\delta_A = \delta_B = 0$. The dashed lines represent a possible behavior after spatial variations are introduced. (a) shear stress; (b) first normal stress difference.

5.3 Elongational Flow

Because of the importance of micellar additives in controlling the extensional rheology of complex fluids employed in consumer applications (eg. paints, shampoos) and in oil recovery, we also examine the predictions of the model in uniaxial elongation.

The steady extensional viscosity is defined as,

$$\eta_E(\dot{\varepsilon}_0) = \frac{\sigma_{zz} - \sigma_{rr}}{\dot{\varepsilon}_0}.$$

In the limit of small extension, ignoring terms of order ϵ, so that $B_{rr} = B_{\theta\theta} = B_{zz} = n_B^0/2$, and taking n_B^0 and n_A^0 at their equilibrium value, Equations (28)-(29) result in

$$\frac{4}{9}\xi^2\dot{\varepsilon}_0^4\eta_E^3 + \frac{2}{3}\xi\dot{\varepsilon}_0^2(2-\dot{\varepsilon}_0)\eta_E^2 + (1+\dot{\varepsilon}_0)(1-2\dot{\varepsilon}_0))\eta_E - 3 + ... = 0. \qquad (42)$$

In linear theory ($\xi = 0$)

$$\eta_E = 3\frac{1}{(1+\dot{\varepsilon}_0)(1-2\dot{\varepsilon}_0)} \qquad (43)$$

and the long chains behave as a single convected Maxwell mode. When $\dot{\varepsilon}_0 = 0$ we have,

$$\eta_E = 3,$$

or, Trouton Ratio $= \eta_E'/\eta_0' = 3$. As we saw before, for large extension rates the two species scission model predicts

$$\eta_E \sim \dot{\varepsilon}_0^{-1.5} \qquad (44)$$

as compared, for example, to Larson's model which predicts

$$\eta_E \sim \dot{\varepsilon}_0^{-1}.$$

The difference arises because of the additional mode of stress reduction arising from scission of the elongated chains in the two species model.

5.4 Parameters

Ultimately we wish to quantitatively compare the model predictions with experimental data. We thus study the effects of varying the equilibrium breaking rate, $c'_{A\text{eq}}$; the equilibrium number density of species B, n_B^0; or the parameter ξ; for the three different types of deformations described above.

5.4.1 Variation on the Equilibrium Breaking Rate

From (33) we see that once the value of λ_{eff} is set by fitting it to SAOS experiments and, once a value of $c'_{A\text{eq}}$ has been chosen, λ_A can be determined from the relationship

$$\lambda_A = \frac{\lambda_{\text{eff}}}{1 - \lambda_{\text{eff}}\, c'_{A\text{eq}}}. \tag{45}$$

Note that for λ_A to remain positive

$$0 \leq c'_{A\text{eq}} \leq \frac{1}{\lambda_{\text{eff}}}.$$

In this section we consider two different limits. In the first limit $c'_{A\text{eq}} << \frac{1}{\lambda_{\text{eff}}}$, hence $\mu \sim 1$, or $\lambda_A \sim \lambda_{\text{eff}}$ since

$$\mu = 1 + c_{A\text{eq}} = \frac{\lambda_A}{\lambda_{\text{eff}}}.$$

So that in this limit $\lambda_{\text{eff}} = \tau_{\text{eff}} \sim \tau_{\text{breaking}} \sim \tau_{\text{reptation}}$. In the second limit, $c'_{A\text{eq}} \sim \frac{1}{\lambda_{\text{eff}}}$ or $\mu > 1$ so that $\tau_{\text{eff}} \sim \tau_{\text{breaking}} << \tau_{\text{reptation}}$.

Figure 7 shows predictions of the damping function for the model in step strain. It can be seen that in the regime where the breaking and reforming rates are large, the damping function is softer. The Lodge-Miessner relation [ref Larson or BB?] asserts that for a step strain γ the first normal stress difference N_1 is related to the shear stress σ by the relationship $N_1(t,\gamma) = \gamma\sigma(t,\gamma)$. In our case, with time-strain factorizability, this becvomes $N_1(\gamma) = \gamma\sigma(\gamma)$. Figure 7 shows that for larger breaking and reforming rates the Lodge-Meissner relation is broken sooner. Experiments have shown that the deviation from that relation, at $\gamma \sim 8$, coincides with the onset of shear banding. In a future paper [13] this phenomenon is studied, and we determine, for a given solution, which of the two limits better agrees the experimental results.

Figure 8 shows the steady shear stress and number density of the longer species as a function of shear rate for different values of the ratio $\mu = \lambda_A/\lambda_{\text{eff}}$. In the limit where $\mu > 1$, such that $c_{A\text{eq}}$ and $c_{B\text{eq}}$ are also large,

the main relaxation mechanism in the intermediate shear-rate region is the breaking and reforming, hence the stress is larger compared to the limit where relaxation is due to both reversible breaking and reptation. Recall that the maximum in the shear stress is a function of the parameters $c_{1\text{eq}}$ and $c_{2\text{eq}}$ as shown in Equation (41). Regardless of the value of μ, the stress contribution from the short species, $B_{r\theta}$, is the same for large $\dot{\gamma}_0$.

In Figure 9, predictions of the model in extensional flow for the two different limiting values of μ are compared with those of Larson's model [35]. As shown in Figure 9a, the model first predicts an increase in the elongational viscosity due to the stretching and alignment of the micellar network segments. However, after an initial increase, the tensile stress difference saturates and the steady elongational viscosity at high rates begins to decrease. Elongational thinning is predicted by our model to be faster than that of Larson's model due to the breaking of the longer, A, species. This decrease in the number of elongated A species at large strains reduces the total tensile stress difference further. For $\xi = 0$ the tensile stress reaches a plateau, corresponding to $\eta_E \sim (\sigma_{zz} - \sigma_{rr})/\dot{\epsilon}_0 \sim \dot{\epsilon}_0^{-1}$, where as for $\xi > 0$ the dominant term in Equation (42, is changed and the steady elongational viscosity decreases at high rates as $\dot{\epsilon}_0^{-1.5}$. Thinning filaments of such fluids would be expected to be Hadamard unstable due to the rapid growth of high wavenumbers disturbances beyond a maximum stress.

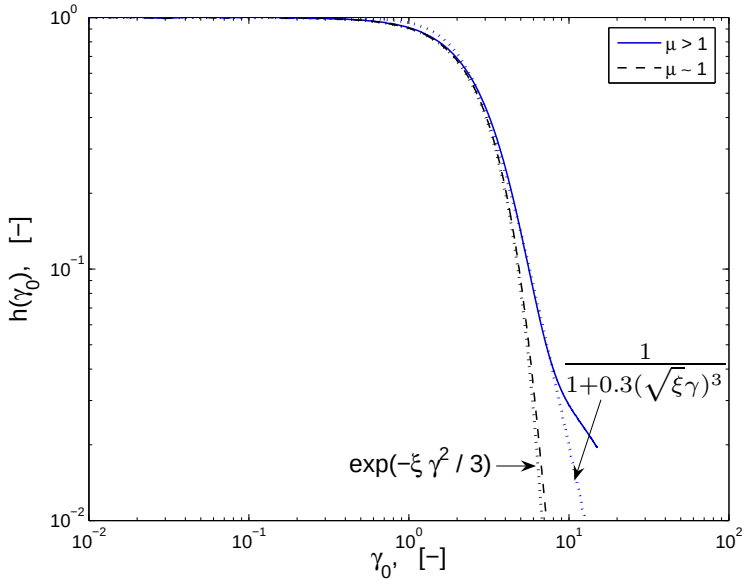

(a)

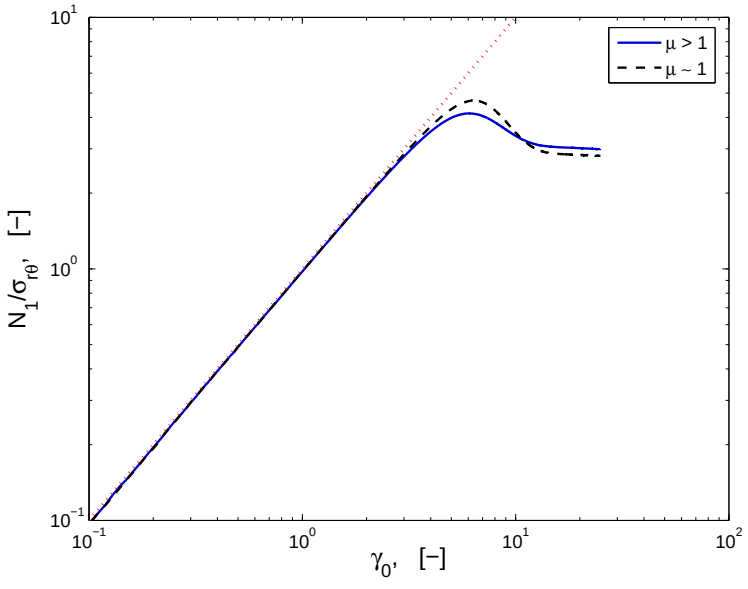

(b)

Figure 7: Model predictions in step strain with variations in μ. (a) damping function, for $\mu \sim 1$ the fit comes from theory and for $\mu > 1$ the fit is numerical; (b) first normal stress difference divided by shear stress, here dotted line demonstrates the extent of agreement with the Lodge-Meissner relation, $N_1/\sigma_{r\theta} = \gamma_0$.

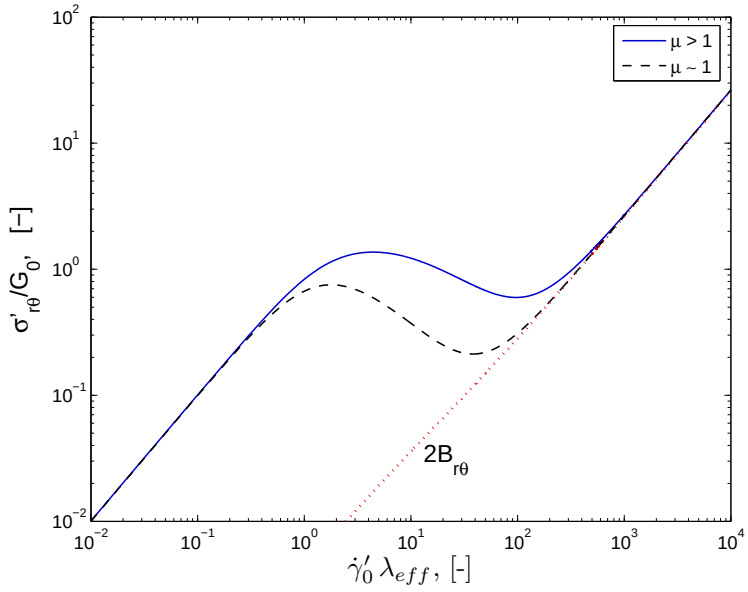

(a)

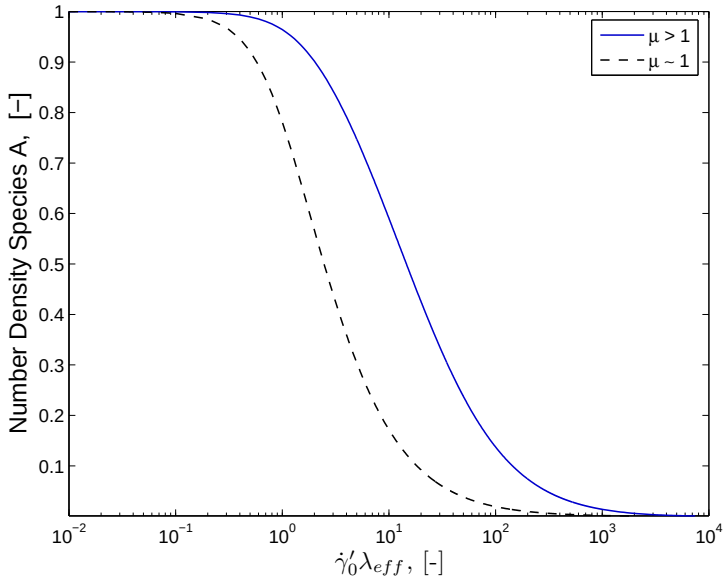

(b)

Figure 8: Model prediction in shear flow for different values of μ. (a) steady shear stress versus shear rate, here the dotted line indicates the contribution to the stress from the short species at large shear rates; (b) number density of species A versus shear rate. The large μ corresponds to $\mu = 3.5$.

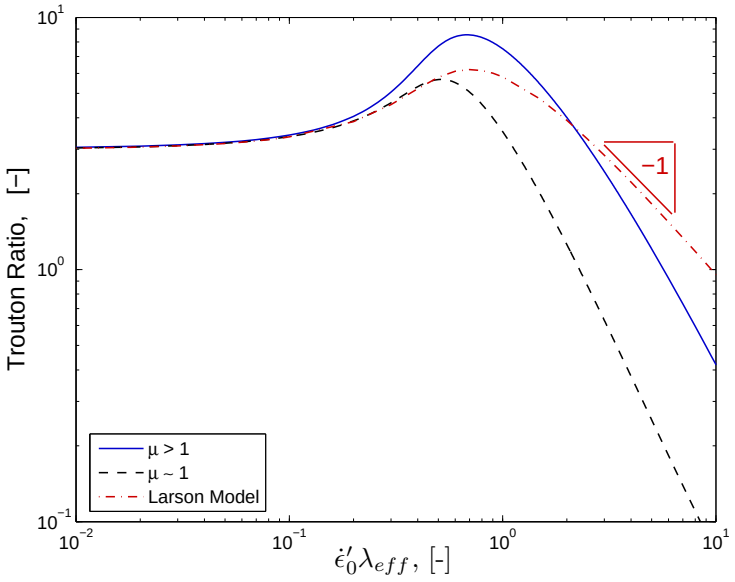

(a)

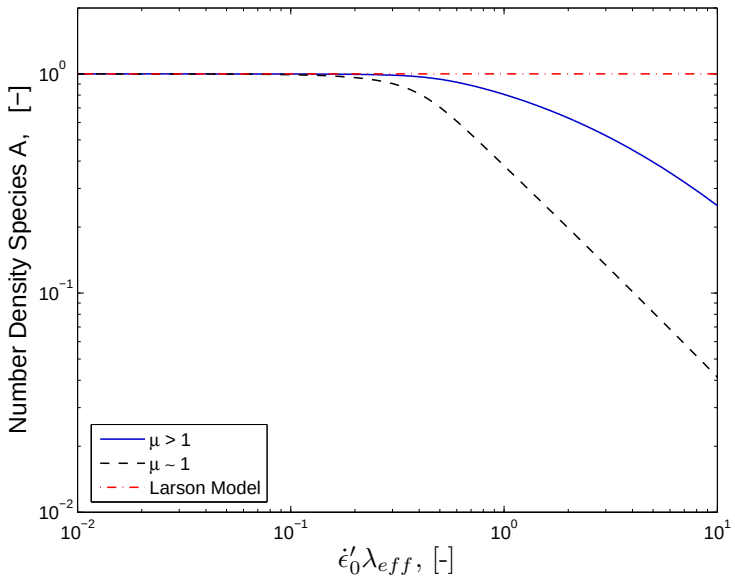

(b)

Figure 9: Prediction of the two species model in elongational flow for different values of μ compared to predictions from the single species Larson model. (a) steady state Trouton ratio versus elongational rate; (b) number density of species A. In this figure, $\xi = 0.3$ for all curves.

5.4.2 Variations of Equilibrium Number Density Species B

In the selection of the parameter n_B^0, note that for the continuous length distribution presented in Cates' theory [45], at equilibrium the micellar length obeys an exponential distribution so that,

$$\frac{n_B^{0'}}{n_A^{0'}} = \frac{\exp\left(\frac{-L/2}{\ell}\right)}{\exp\left(\frac{-L}{\ell}\right)}$$

or, with our non-dimensionalization (based on $n_A^{0'}$) we find,

$$n_A^0 = 1, \qquad n_B^0 = \exp\left(\frac{L/2}{\bar{\ell}}\right) \tag{46}$$

where $\bar{\ell}$ is the "average" length of the micelles. If $n_B^0 = e^\kappa$, this corresponds to choosing the length of the short chains to be κ-times the average length as it is understood in Cates theory. Thus bigger κ implies longer chains relative to $\bar{\ell}$. In this study we have chosen $\kappa = 1, 1/2, 1/8$. Figure 10 shows the damping function plotted for different values of n_B^0. It can be seen that if the length of species A, at equilibrium, is longer than the average length, i. e. $\kappa \sim 1$, after a deformation is applied species A will break at smaller strains than when $\kappa < 1$. In shear flow, the maximum in the intermediate shear rate region of the curve of steady shear stress versus shear rate is higher for smaller κ because species A break faster. The dependence of the maximum on the shear stress is given by Equation (41). The curve of steady shear stress versus shear rate is unaffected in the non-monotonic regions. In extensional flow, smaller values of κ result in a larger elongational thickening. In this section, plots of the viscometric properties of shear and elongational flows are omitted since the variations, as n_B^0 changes, are qualitatively similar to that in Figures 8 and 9.

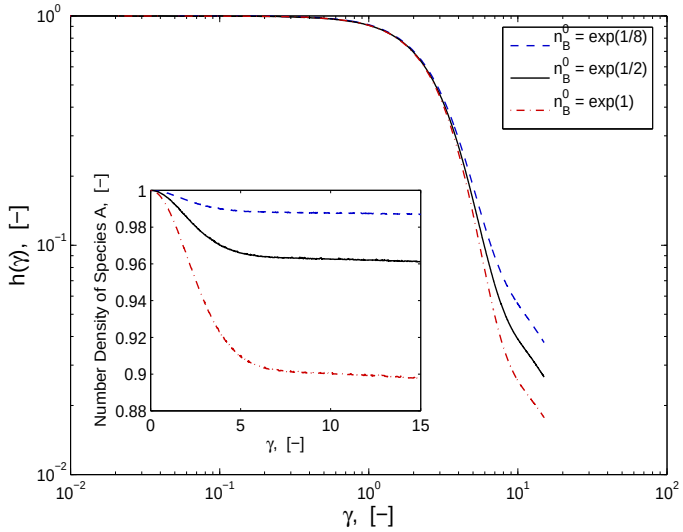

Figure 10: Model prediction of damping function versus applied strain for different n_B^0. Insert: Breaking of chains of length L as function of applied strain.

5.4.3 Variations of the Partially-Extending Strand Parameter ξ

Recall from Section 2.3 that the long species, A, break according to

$$c_A = \frac{1}{3}\xi\mu\left(\dot{\gamma} : \frac{\mathbf{A}}{n_A}\right) + c_{A\text{eq}},$$

hence variations on the parameter ξ directly affect the breaking rate as a function of the strain, shear rate, and elongational rate. As a consequence, smaller values of ξ result in a softer damping function, larger steady-state shear stress, and bigger elongational thickening, as seen in Figures 11, 12.

The value of the parameter ξ necessary to predict experimental responses of a given solution will be found by fittings to step strain experiments, since this parameter directly affects the strain hardening.

In Figure 11a, the damping function as predicted by our model is compared to results using Equation (40). Predictions for strains larger than 5 are studied in a future paper [28], since the onset of shear banding has been observed for strains of this order [13]. In Figure 11b, it is shown that the model output agrees with the Lodge-Meissner relation up to a strain value dependent on the value of the parameter ξ, with agreement up to higher values of γ for smaller ξ as anticipated.

In Figure 12a the dependence of the shear stress as a function of the shear rate, and in Figure 12b the dependence of the Trouton ration on the extension rate, as ξ varies, are shown. As anticipated as ξ goes to zero, the shear stress approaches a monotone (upper convected Maxwell like) dependence on the shear rate, and the Trouton ration approaches an unbounded curve at finite extensions rate (again Maxwell like). Once regularized by ξ the Trouton ration shows a maximum followed by a decreasing curve behaving like $\dot{\epsilon}^{-1.5}$.

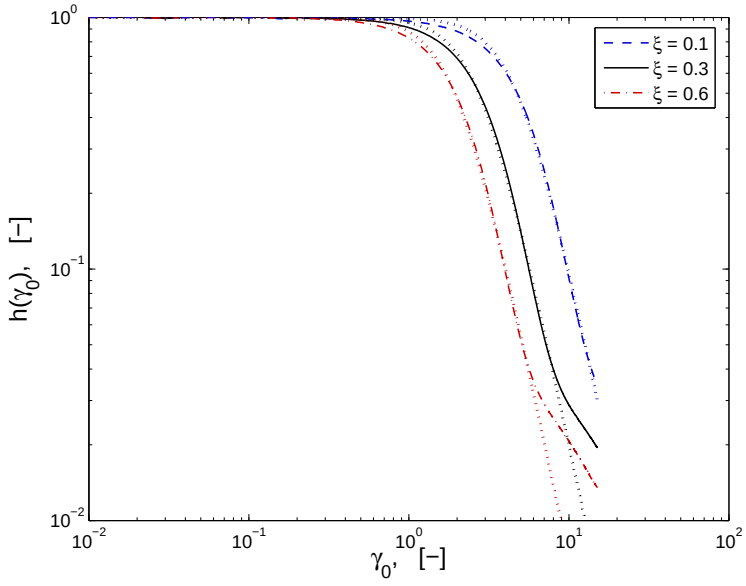

(a)

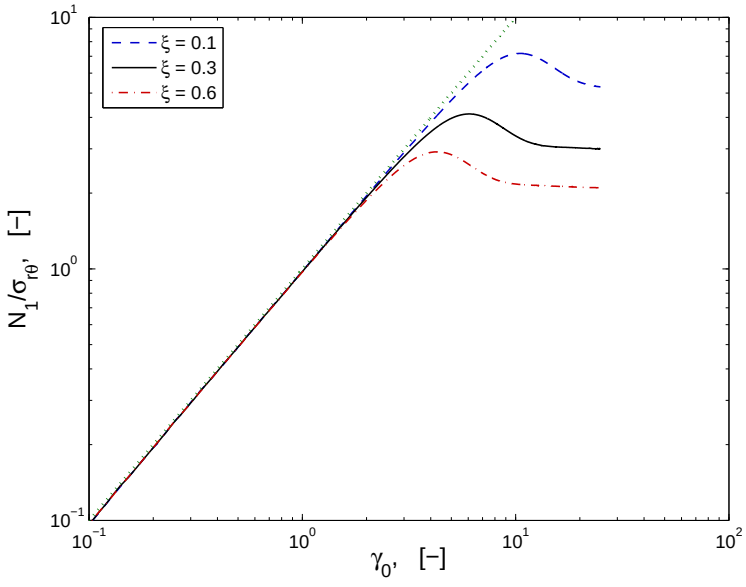

(b)

Figure 11: Model prediction in step strain for different values of ξ. (a) Damping function versus applied strain; (b) Lodge-Meissner Relation.

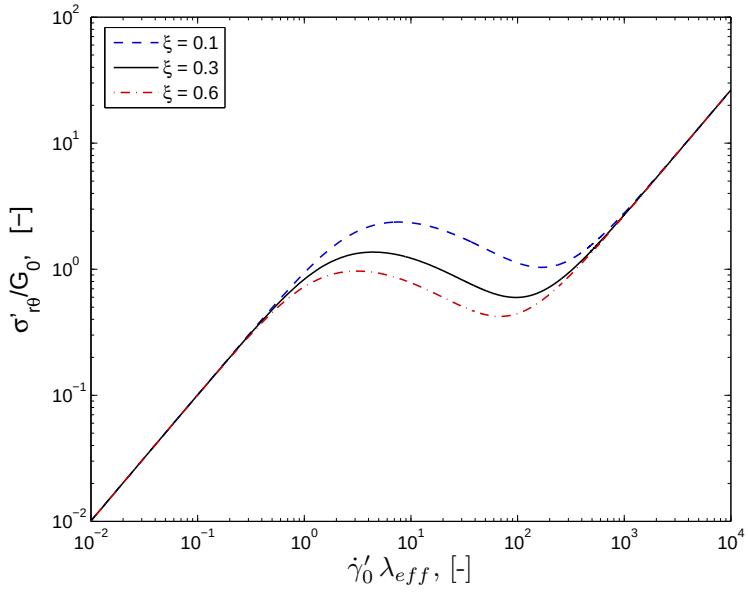

(a)

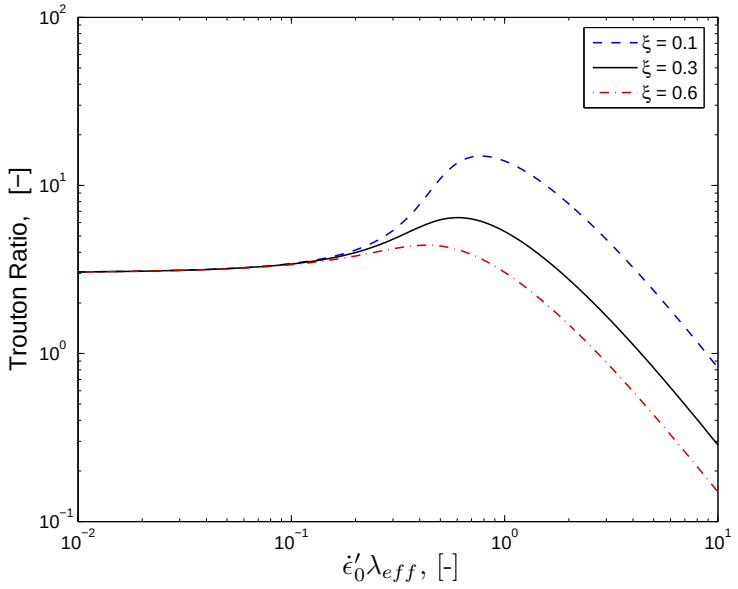

(b)

Figure 12: Model predictions in shear and elongational flow for different values of the parameter ξ. (a) steady state shear stress versus shear rate; (b) steady state Trouton ratio versus elongational rate.

6 Transient Response

As discussed before, predictions from the model under homogenous flow are only valid in regions where the spatial variation of the number densities of the species are not important, that is regions where there is not shear banding. Experiments with a 100nM CpyCl solution have shown that, for this solution, shear banding begins at a strain of about 8 [13], hence predictions assuming homogenous flow are only valid up to strains of this order. Figure 13 shows the model predictions in transient shear flow for variations of the parameter ξ at a constant shear rate $\dot{\gamma}_0 = \dot{\gamma}'_0 \lambda_{\text{eff}} = 1$, the insert shows the variations of the number density of species A. Figure 14 shows the transient predictions of the model for different shear rates, the stress are plotted up to strains of 8. Continuation of such curves to steady state, that will correspond to experimental results, need to be done after diffusion is reincorporated into the equations.

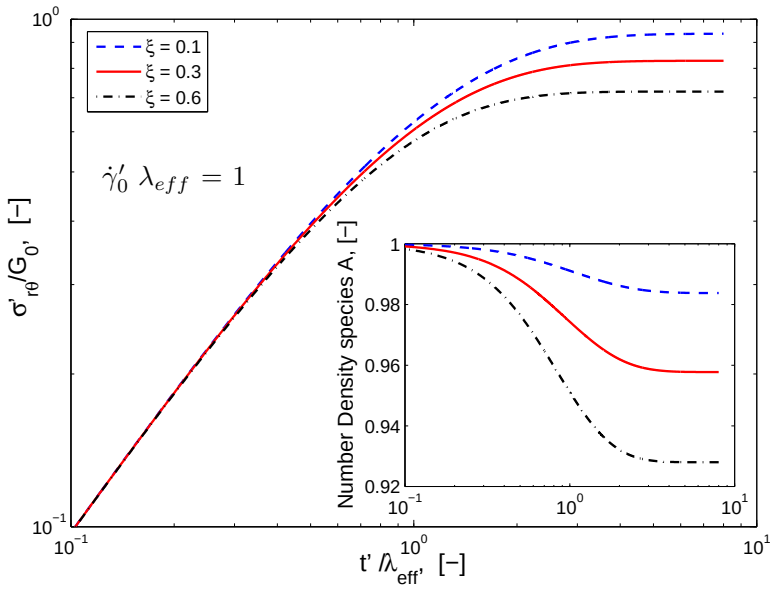

Figure 13: Model predictions in transient shear flow for different values of the parameter ξ. Insert: Variationof the number density of species A in time. Here $\lambda_{\text{eff}} = 1.17$ s and $G_0 = 27$ Pa.

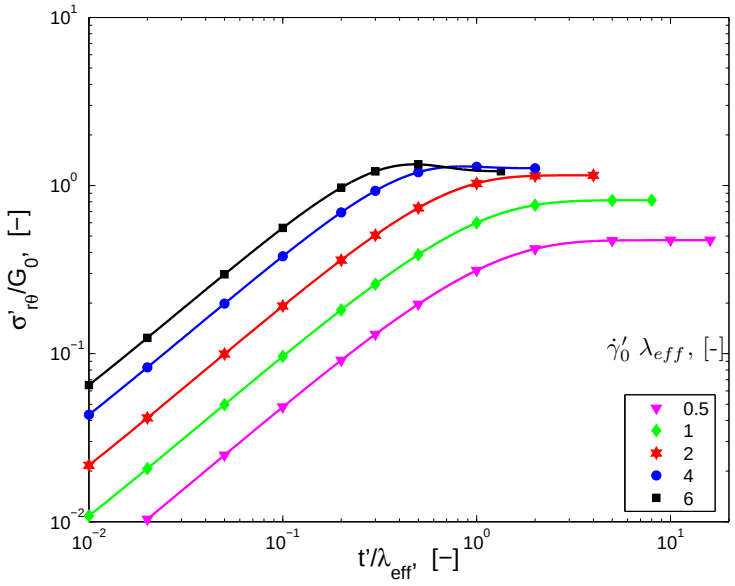

(a)

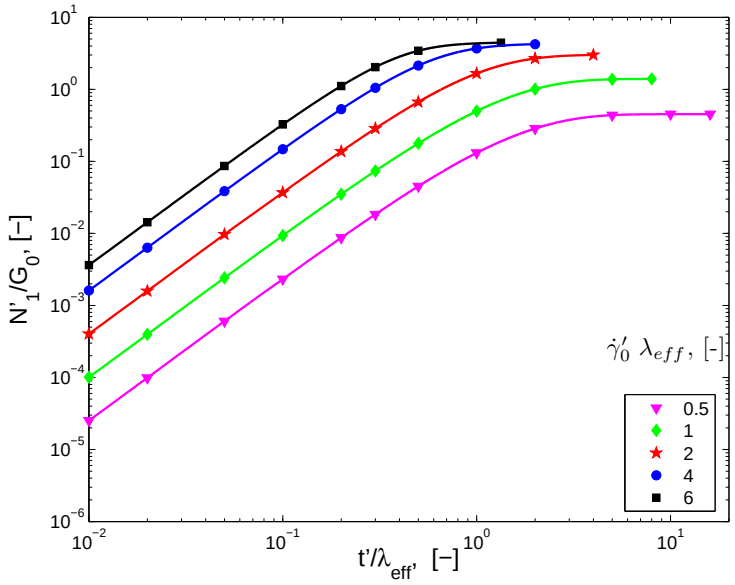

(b)

Figure 14: Model predictions in shear in transient shear flow for different shear rates. Here $\lambda_{\text{eff}} = 1.17$ s and $G_0 = 27$ Pa. (a) shear stress versus time; (b) first normal stress difference versus time.

7 Conclusion

We have presented a model for wormlike micellar solutions involving scission and reforming of chains based on non-affine network theory and a discrete version of Cates theory. Specifically, we consider two elastically active species long chains which are convected by the flow and undergo rupture at a rate that depends on the deformation rate and on the local elongation rate. Following rupture the new shorter elastic chains partially retract before being reconnected to the network. This partially-extended and convected (PEC) response is captured by a single nonlinear model parameter ξ which controls the level of extension thickening in elongation and of strain softening in step strain displacements. To date we have only considered Hookean elastic segments, however it is straightforward to consider numerically the role of nonlinear (FENE) springs [19]. We anticipate that this will result in strain-hardening at intermediate shear strains, as observed by Brown *et. al.* [12], and a further enhancement in the extension thickening expected in uniaxial elongation. The model, which allows for inhomogeneities in the flow, was examined in various flow situations, steady state circular Couette shear flow, step strain, extension, and linear small angle oscillatory flow. The effects the parameters of the model have on the flow are shown. In future papers [13] the model predictions will be compared directly with experiment and in [28] the full inhomogeneous flows are computed.

The authors thank N. J. Kim, C. Pipe, J. Rothstein, E.Miller and L. Zhou for many helpful discussions.

This work was supported by grant NSF-DMS #0405931.

References

[1] M.E. Cates and S.J. Candau. Statics and dynamics of worm-like surfactant micelles. *J. Phys.: Condens. Matter*, 2:6869–6892, 1990.

[2] P. Olmsted. Dynamics and flow-induced phase separation in polymeric fluids. *Current opinion in colloid and interface science*, 4(2):95–100, April 1999.

[3] H. Rehage and H. Hoffmann. Viscoelastic surfactant solutions: Model systems for rheological research. *Molecular Physics*, 74:933–973, 1991.

[4] M.S. Turner and M.E. Cates. Linear viscoelasticity of wormlike micelles - a comparison of micellar reaction-kinetics. *J.Phys. II France*, 2:503–519, 1992.

[5] M.E. Cates. Flow behavior of entangles surfactant micelles. *J. Phys.: Condens. Matter*, 8:9167–9176, 1996.

[6] M.E. Cates. Nonlinear viscoelasticity of wormlike micelles (and other reversibly breakable polymers). *J. Phys. Chem.*, 94:371–375, 1990.

[7] G. Porte, J-F. Berret, and J.L. Harden. Inhomogeneous flows of complex fluids: Mechanical instability versus non-equilibrium phase transition. *J. Phys. II France.*, 7:459–472, 1997.

[8] Y.T. Hu and A. Lips. Kinetics and mechanism of shear banding in entangled micellar solutions. *J. Rheol.*, 49(5):1101–1027, 2005.

[9] J.P. Rothstein and E. Miller. Private communications, 2005.

[10] J.B. Salmon, A. Colin, S. Manneville, and F. Molino. Velocity profiles in shear-banding wormlike micelles. *Phys. Rev. Letters*, 90:228303–1 – 228303–4, 2003.

[11] R.K. Prud'homme and G.G. Warr. Elongational flow of solutions of rodlike micelles. *Langmuir*, 10:3419–3426, 1994.

[12] E.F. Brown, W.R. Burghardt, and D.C. Venerus. Tests of the Lodge-Meissner relation in anomalous nonlinear step strain of an entangled wormlike micelle solution. *Langmuir*, 13:3902=3904, 1997.

[13] C.J. Pipe, N.J. Kim, G.H. McKinley, P.A. Vasquez, and L.P. Cook. Wormlike micellar solutions II: Comparison between experimental data and scission model predictions. *Preprint.*

[14] M.E. Cates. Reptation of living polymers: Dynamics of entangled polymers in the presence of reversible chain-scission reactions. *Macromolecules*, 20:2289–2296, 1987.

[15] J-F. Palierne. Sticky dumbbells: from Hookean dumbbells to transient network. *Rheol. Acta*, 36:534–543, 1997.

[16] J.G. Hernandez-Cifre, Th. M.A.M. Barenburg, J.D. Schieber, and B.H.A.A. van den Brule. Brownian dynamics simulation of reversible polymer networks under shear using a non-interacting dumbbell model. *J. Non-Newt. Fluid Mech.*, 113:73–96, 2003.

[17] F. Bautista, J.F.A. Soltero, J.H. Perez-Lopez, J.E. Puig, and O. Manero. On the shear banding flow of elongated micellar solutions. *J. Non-Newt. Fluid Mech.*, 94:57–66, 2000.

[18] B.H.A.A. van den Brule and P.J. Hoogerbrugge. Brownian dynamics simulation of reversible polymeric networks. *J. Non-Newt. Fluid Mech.*, 60:303–334, 1995.

[19] A. Tripathi, K.C. Tam, and G.H. McKinley. Rheology and dynamics of associative polymers in shear and extension: theory and experiments. *Macromolecules.*, 39:1981–1999, 2006.

[20] P.D. Olmsted, O. Radulescu, and C.-Y.D. Lu. Johnson-Segalman model with a diffusion term in cylindrical Couette flow. *J. Rheol*, 44(2):257–275, March/April 2000.

[21] C. Y D. Lu, P. D. Olmsted, and R. C. Ball. Effects of nonlocal stress on the determination of shear banding flow. *Phys. Rev. Ltrs.*, 84 4 Jan.:642–645, 2000.

[22] O. Radulescu and P. D. Olmsted. Matched asymptotic solutions for the steady banded flow of the diffusive Johnson-Segalman model in various geometries. *J of Non-Newt Fluid Mech.*, 91:143–164, 2000.

[23] L.P. Cook and L.F. Rossi. Shear layers and demixing in a model for shear flow of self-assembling micellar solutions. *Journal Non-Newt. Fluid. Mech*, 116:347–369, 2004.

[24] L.F. Rossi, G.H. McKinley, and L.P. Cook. Slippage and migration in taylor-couette flow of a model for dilute wormlike micellar solutions. *J. Non-Newt. Fluid Mech.*, 136:79–92, 2006.

[25] R.G. Larson. *Constitutive Equations for Polymer Melts and Solutions*. Butterworths Series in Chemical Engineering, ed. H. Brenner. Butterworths, Boston, 1988.

[26] R.W. Mair and P.T. Callaghan. Shear flow of wormlike micelles in pipe and cylindrical Couette geometry as studied by nuclear magnetic resonance microscopy. *J. Rheol.*, 41:901–924, 1997.

[27] M.W. Liberatore, F. Nettlesheim, N.J. Wagner, and L. Porcar. Spatially resolved small-angle neutron scattering in the 1-2 plane: A study of shear induced phase-separating wormlike micelles. *Phys. Rev. E*, 73:20504–1–20504–4.

[28] L. Zhou, L.P. Cook, P.A. Vasquez, and G.H. McKinley. Wormlike micellar solutions III: Inhomogeneous flow predictions of scission model.

[29] P. D. Olmstead and C. Y. D. Lu. Co-existence and phase separation in sheared complex fluids. *Phys. Rev. E*, 56:56–59, 1997.

[30] R.B. Bird, C.F. Curtiss, R.C. Armstrong, and O. Hassager. *Dynamics of Polymeric Liquids: Vol 2, Kinetic Theory*. John Wiley and Sons, New York, second edition, 1987.

[31] A.N. Beris and V.G. Mavrantzas. On the compatibility between various macroscopic formalisms for the concentration and flow of dilute polymer solutions. *J. Rheol.*, 38(5):1235–1250, Sept/Oct 1994.

[32] A.V. Bhave, R.C. Armstrong, and R.A. Brown. Kinetic theory and rheology of dilute, non-homogeneous polymer solutions. *Chem. Phys.*, 95(14) August:2988–3000, 1991.

[33] M. Doi and S.F. Edwards. *The Theory of Polymer Dynamics*. Oxford University Press, 1986.

[34] R.G. Larson. *The Structure and Rheology of Complex Fluids*. Oxford University Press, New York, 1999.

[35] R.G. Larson. A constitutive equation for polymer melts based on partially extending strand convection. *J. Rheol.*, 28:545–571, 1984.

[36] G. Marrucci, F. Greco, and G. Iannurberto. Integral and differential constitutive equations for entangled polymers in simple versions of ccr and force balance in entanglement. *Rheol. Act.*, 40:98–103, 2001.

[37] A.E. Likhtman and R.S. Graham. Simple constitutive equation for linear polymer melts derived from molecular theory: Rolie-poly equation. *J. Non-Newt. Fluid Mech.*, 114(1):1–12, September 2002.

[38] S.A. Khan and R.G. Larson. Comparison of simple constitutive equations for polymer melts in shear and biaxial and uniaxial extensions. *J. Rheol.*, 31:207–234, 1987.

[39] A. Bhardwaj, E. Miller, and J.P. Rothstein. Filament stretching and capillary breakup extensional rheometry measurements of visocelastic wormlike micelle solutions. *Submitted for publication*.

[40] M.W. Liberatore, F. Nettlesheim, E.W. Kaler, N.J. Wagner, and Y.T. Hu. Shear banding and shear thinning in solutions of wormlike micelles, part I: Flow kinematics by particle tracing velocimetry. *preprint*.

[41] M.W. Liberatore, F. Nettlesheim, E.W. Kaler, N.J. Wagner, T. Nu, and L. Porcar. Characterization of solutions of wormlike micelles underflow: Microstructure and investigations in the 1-2 plane. *preprint*.

[42] D. Varade, T. Joshi, V.K. Aswal, P.S. Goyal, P.A. Hassan, and P. Bahadur. Effect of salt on the micelles of cetyl pyridinium chloride. *Colloid. and Surfaces A: Physicochem. Eng. Apects*, 259:395–101, 2005.

[43] P. Fischer and H. Rehage. Non-linear flow properties of viscoelastic surfactant solutions. *Rheol. Acta*, 36:13–27, 1997.

[44] J.F. Berret, D. C. Roux, and G. Porte. Isotropic-to-nematic transition in wormlike micelles under shear. *J. Phys. II (France))*, 4:1261–1279, 1994.

[45] M.E. Cates. Reptation of living polymers: Dynamics of entangled polymers in the presence of reversible chain-scission reactions. *Macromolecules*, 20:2289–2296, 1987.